DEVELOPMENT OF A MICROWAVE-BASED BIOSENSOR TO DETECT ANTI-P53 ANTIBODIES AS A BIOMARKER FOR EARLY DETECTION OF COLORECTAL CANCER

Sebastian Montoya Villada

Instituto Tecnológico Metropolitano
Facultad de Ingenierías
Medellín, Colombia
2025

DEVELOPMENT OF A MICROWAVE-BASED BIOSENSOR TO DETECT ANTI-P53 ANTIBODIES AS A BIOMARKER FOR EARLY DETECTION OF COLORECTAL CANCER

Sebastian Montoya Villada

Thesis presented as a partial requirement for obtaining the degree of:
Magister en Automatización y Control Industrial

Director (a):
Ph.D. Erick Estefen Reyes Vera

Director (a):
Ph.D. Jahir Orozco Holguín

Línea de Investigación:
Visión Artificial y Fotónica
Grupo de Investigación:
Automática, Electrónica y Ciencias Computacionales

Instituto Tecnológico Metropolitano
Facultad de Ingenierías
Medellín, Colombia
2025

(Dedicatoria o lema)

Acknowledgment

I would like to express my sincere gratitude to my tutor, Jahir Orozco Holguín, for his invaluable guidance, expertise, and encouragement, which were crucial throughout this journey. I am equally thankful to my tutor and friend, Erick Reyes Vera, for his steadfast support, insightful advice, and camaraderie, which made this process both enriching and fulfilling.

I extend my heartfelt appreciation to my supervisor, Nelson Darío Gómez Cardona, for his trust and for providing me with opportunities that fostered personal and professional growth. To my family and friends, thank you for your unwavering love, patience, and belief in me, which gave me the strength to overcome every obstacle.

My deepest thanks go to the staff of the Polymer Materials Laboratory, whose support, collaboration, and expertise were instrumental in addressing challenges and achieving the goals of this project. I also wish to acknowledge the ITM for its invaluable resources, knowledge, and opportunities, which were fundamental to the development of this work.

I acknowledge Dr. Luis Gerónimo Restrepo and Dr. Nestor Llinás from Fundación Colombiana de Cancerología Clínica Vida, Medellín, Colombia, who kindly donated serum samples, and Dr. Andrés Felipe Cruz Pacheco and Yeisson Monsalve from the Max Planck Tandem Group in Nanobioengineering at the University of Antioquia and Camilo Zapata Hernandez from ITM, for technical assistance.

Abstract

Colorectal cancer (CRC) remains a leading cause of morbidity and mortality worldwide, with early detection playing a critical role in improving patient outcomes. This thesis develops a label-free microwave-based biosensor for detecting anti-p53 antibodies, a biomarker of early CRC. The biosensor employs a transduction mechanism in the microwave region based on stepped impedance resonators integrated into a microstrip line, enabling precise dielectric permittivity measurements and facilitating the detection of biomolecular interactions. The biosensor utilizes a 3,3′-Dithiodipropionic acid di(N-hydroxysuccinimide ester) (DTSP) self-assembled monolayer to covalently immobilize p53 proteins on the sensor surface, ensuring high specificity and sensitivity.

Analytical evaluations revealed a linear working range from 0 to 1250 pg/mL and a detection limit of 315.29 pg/mL, making it clinically relevant for early CRC diagnosis. Cross-reactivity studies demonstrated the biosensor's exceptional specificity and selectivity, distinguishing anti-p53 antibodies from potential interferents such as cytokines, antibodies, and small molecules. The biosensor's performance was further validated against the gold-standard ELISA method, achieving a strong correlation with a 0.97 correlation coefficient. Recovery rates of 87.2 to 97.2% and relative standard deviations between 1.5 and 4.3% highlight the biosensor's accuracy and reproducibility. Likewise, stability assessments confirmed consistent performance over two weeks, with minimal variation, underscoring the robustness of the biosensing surface.

This master thesis demonstrates that the proposed microwave-based biosensor is a robust, efficient, and cost-effective platform for detecting anti-p53 antibodies. It represents a significant advancement in biosensor technology, offering a practical and accessible solution for early cancer diagnostics and contributing to the broader field of biomedical sensing. The use of cost-effective copper-based materials, combined with the simplicity and scalability of the microwave technology, underscores the biosensor's potential for point-of-care applications. Its compact design, rapid detection capabilities, and compatibility with decentralized diagnostic systems make it a promising tool for improving CRC screening, particularly in resource-limited settings. Future work will focus on expanding the biosensor's applicability to additional biomarkers and refining its integration into clinical workflows.

Keywords: Colorectal cancer, Anti-p53 antibodies, Microwave-based biosensor, Label-free detection, Point-of-care diagnostics, Biosensing

Content

List of Figures

List of Tables

List of Acronyms

Symbol	Térm	SI unit
W	Total width of the substrate	mm
L	Total length of the substrate	mm
w_1	Width of the microstrip line	mm
l_p	Length of the patch	mm
w_p	Width of the patch	mm
g	Gap between the line and the patch	mm
l_g	Length of the gap	mm
ε_r	Relative dielectric constant	
h	Substrate height	*mm*
f_R	Resonance frequency	GHz
S_{21}	Transmission coefficient	dB
C	Capacitance	pF
L	Inductance	nH
Δf	Frequency shift	MHz
λ	Wavelength	nm
$Z0$	Reference impedance	Ω
k_c	Cutoff wavenumber	rad/m
a,b	Waveguide dimensions	mm
R^2	Correlation coefficient	
pv	p-value (statistical significance)	
F	F-statistic (ANOVA)	
AA	Ascorbic acid	mg/mL
IL-6	Interleukin-6	pg/mL
PBS	Phosphate-buffered saline	
BSA	Bovine Serum Albumin	%
DTSP	3,3′-Dithiodipropionic acid di(N-hydroxysuccinimide ester)	mM
CCR	Colorectal cancer	
p53	Tumor suppressor protein	ng/mL
ANOVA	Analysis of Variance	
IgG	Immunoglobulin G	pg/mL
S/N	Signal-to-noise ratio	
LOD	Limit of detection	pg/mL
IL-8	Interleukin-8	pg/mL
β−1,4−Gal−TIV	β-1,4-galactosyltransferase IV	pg/mL

1. Introduction

Cancer is a complex disease that affects millions of people worldwide and remains one of the primary areas of focus for the scientific community in its efforts toward treatment and control. It is among the leading causes of death globally, with its incidence continuing to rise (Bray Bsc et al., 2024; Li & Kuang, 2024). Cancer occurs when normal body cells become abnormal and start dividing uncontrollably, forming benign or malignant tumors (Boutry et al., 2022; Wang et al., 2021). Benign, non-cancerous tumors tend to remain localized and generally do not spread to other parts of the body. In contrast, malignant, cancerous tumors can invade other regions of the body, posing a potentially lethal threat (Patel, 2020). Several factors can increase the risk of developing cancer, including exposure to environmental agents such as radiation and pollution, lifestyle choices such as smoking, alcohol consumption, obesity, and genetic predisposition (Irigaray et al., 2007; Rahman et al., 2018).

According to data collected by the Global Cancer Observatory (GLOBOCAN) and provided by the World Health Organization (WHO) in 2020, breast, lung, colorectal, prostate, and stomach cancer are the most prevalent types globally. Among these, CRC stands out as the third most diagnosed cancer worldwide. However, its high survival rate makes it a crucial target for early detection. In 2022, an estimated 151,030 adults in the U.S. were diagnosed with CRC. Of these, 106,180 were new cases of colon cancer (54,040 men and 52,140 women), and 44,850 were new cases of rectal cancer (26,650 men and 18,200 women). The 5-year survival rate for individuals with localized CRC was 91%, while For patients with colorectal cancer in an intermediate stage (when it has spread to nearby lymph nodes), it was 72%. It highlights the critical importance of early cancer detection at different stages of progression.

According to the Ministry of Health, from 4,771 new cancer cases detected in Colombia by the end of 2021, CRC showed high incidence rates in both genders, with 168 cases in men and 195 cases in women. This led to 59 deaths in men and 47 in women, primarily affecting adults over 65 years old (Instituto Nacional de Cancerología-ESE, 2020). CRC is often diagnosed at advanced stages, and 50% of patients experience delays of up to 32 days in receiving a diagnosis, which can negatively affect the prognosis and treatment effectiveness (Minsalud, 2021). In contrast, early cancer diagnosis offers numerous benefits, including a more effective and less invasive treatment with a significant reduction in the overall cost (Piñeros et al., 2022). In this regard, the development of Point-of-Care (POC) tests, which are cost-effective, user-friendly, and provide rapid disease diagnoses, is gaining attention to expedite CRC diagnosis. Furthermore, POC systems could be implemented in decentralized diagnostic settings in rural areas and underserved regions where specialized equipment and medical personnel are limited, significantly improving access to healthcare.

Diagnosis and monitoring of CRC is based on biomarker detection, providing valuable information about the cancer's status and aiding in timely diagnosis and proper treatment. Some of the most commonly used biomarkers in CRC detection include carcinoembryonic antigen (CEA), microtubule-associated protein kinase (MAP), p16INK4a protein, TMPRSS2-ERG fusion protein, β-1,4-galactosyltransferase-V enzyme, carbohydrate antigen (CA-19-9), and p53 protein (Sundarraj et al., 2022). From them, detecting anti-p53 antibodies has garnered significant interest for early CRC diagnosis. The p53 gene is a tumor suppressor gene found in the DNA of cells, and its mutation or absence is directly associated with the development of several types of cancer, including CRC. The detection of anti-p53 antibodies can be helpful, as their presence has been linked to the onset, progression, and prognosis of CRC. POC tests that focus on detecting biomarkers like anti-p53 antibodies offer a valuable tool in diagnosing this disease, thereby improving treatment success rates and patient survival.

POC systems incorporate biosensors for the highly sensitive and specific detection of biomarkers, minimizing nonspecific responses to proteins, antibodies, lipids, and other components in clinical samples that may cause interference. Biosensors are compact-size devices that use specific biochemical reactions mediated by isolated enzymes, components of the immune systems, tissues, organelles, or whole cells (Bijalwan et al., 2021; Guthula et al., 2022; Lee et al., 2013; Yılmaz et al., 2021) to detect (bio)chemical compounds, typically through electrical, piezoelectric, thermal, or optical transduction signals (Proudfoot et al., 2011). Such output signals correlate well with changes in target analyte concentration and are easy for non-specialized personnel and users to interpret. Recent biosensor research and development advancements aim to real-time measurements to analyze samples quickly, precisely, and efficiently with small sample quantities (Berketa et al., 2022; Bourjilat et al., 2016; Gul et al., 2022; Khalid et al., 2018; Lee et al., 2013; Mehrotra et al., 2019a; Menzler et al., 2022; Rocchitta et al., 2016; Sharif et al., 2023; Su et al., 2013).

Sensors using microwave technology are key tools in automation and industrial control due to their ability to accurately and in real-time measure the presence of substances in samples through changes in their dielectric permittivity (Acevedo-Osorio et al., 2020; Reyes-Vera et al., 2019; Zapata-Londoño et al., 2021). However, in biomedical diagnosis, measuring only changes in dielectric permittivity is insufficient, as many pathologies are associated with the overexpression of biomarkers that can affect it. Developing biosensors based on microwave technology offers a promising detection alternative. This technology can achieve sufficient sensitivity to detect biomolecules, enabling rapid, real-time detection. Additionally, it is non-invasive and versatile, allowing for the detection of a wide range of biomolecules without affecting biological samples or requiring additional signal amplification. It is also relatively cost-effective and scalable compared to more sophisticated technologies like fiber optics, integrated optics, or Micro-Electro-Mechanical Systems (MEMS). This technology has demonstrated its ability to manufacture highly robust, repeatable, precise, sensitive biosensors with a high-quality factor (Amanati Shahri et al., 2022; Ebrahimi et al., 2020; Kai Boon et al., 2021; Lee et al., 2013; Mehrotra et al., 2019b; Wu, 2016) making it suitable for

commercial applications and the development of disease monitoring and control systems in low- or middle-income settings such as Colombia.

The objective of this master's thesis was to develop a microwave-based biosensor to detect anti-p53 antibodies as a biomarker for the early detection of CRC. A microwave-based transducer platform was functionalized with p53 protein bioreceptors to detect anti-p53 antibodies. The functional platform was optimized for analytical performance to determine sensitivity, selectivity, linearity range, detection limits, reproducibility, and stability. The optimized microwave-based biosensor response was interrogated in samples from patients diagnosed with CRC and compared with those from healthy individuals to demonstrate the potential of the device technology for CRC biomarker detection. In this context, implementing a microwave-based biosensor to detect anti-p53 antibodies could significantly impact the early detection of CRC as an enhanced control and automation system in the biomedical industry.

1.1 Motivation

The need for rapid and reliable detection methods in the medical field, particularly in cancer diagnosis, has grown significantly in recent years. Colorectal cancer, one of the most prevalent cancers worldwide, can be more effectively treated when detected early. Identifying specific biomarkers, such as anti-p53 antibodies, plays a crucial role in early detection, enabling healthcare professionals to diagnose and monitor the progression of the disease.

While there have been advancements in the development of diagnostic tools for CRC, integrating novel sensor technologies that offer fast, sensitive, and non-invasive detection methods remains a key area of research. Microwave-based biosensors, particularly those based on microstrip technology, represent a promising approach to detecting cancer biomarkers, such as anti-p53 antibodies. This research is motivated by the need to create more efficient and accessible diagnostic tools for CRC detection, focusing on using innovative sensor technologies to enhance early diagnosis and improve patient outcomes.

1.2 Objectives

1.2.1 General Objective

To develop a microwave-based biosensor based on microstrip technology for detecting anti-p53 antibodies as colorectal cancer (CRC) biomarker.

1.2.2 Specific Objectives

SO1: To develop a microwave-based transducer for identifying biological substances through dielectric permittivity measurements.

SO2: To design and test a methodology for functionalizing the transducer to specifically and sensitively detect anti-p53 antibodies.

SO3: To evaluate the analytical properties of the developed biosensors for detecting anti-p53 antibodies in terms of linear working range, sensitivity, specificity, detection limits, and stability.

SO4: To compare the response of the developed biosensors with a standard technique for detecting anti-p53 antibodies.

2. Theoretical Background

2.1 Colorectal Cancer and Its Diagnosis

2.1.1 Development of Colorectal Cancer

Oncological studies investigate the treatment of CRC in the different stages of development within the body. Most CRC cases begin as polyps, with adenomatous polyps and hyperplastic polyps being the most common types. These growths are considered precancerous lesions that form in the inner layers of the colon or rectum, as shown in Figure 2-1. While hyperplastic polyps are benign and do not pose a health threat, adenomatous polyps consist of abnormal cells with a higher potential to become cancerous as they grow. Early detection and removal of adenomatous polyps are critical to preventing progression to CRC and improving patient prognosis. In this context, regular screening exams, such as colonoscopy, play a crucial role in the prevention and early detection of CRC.

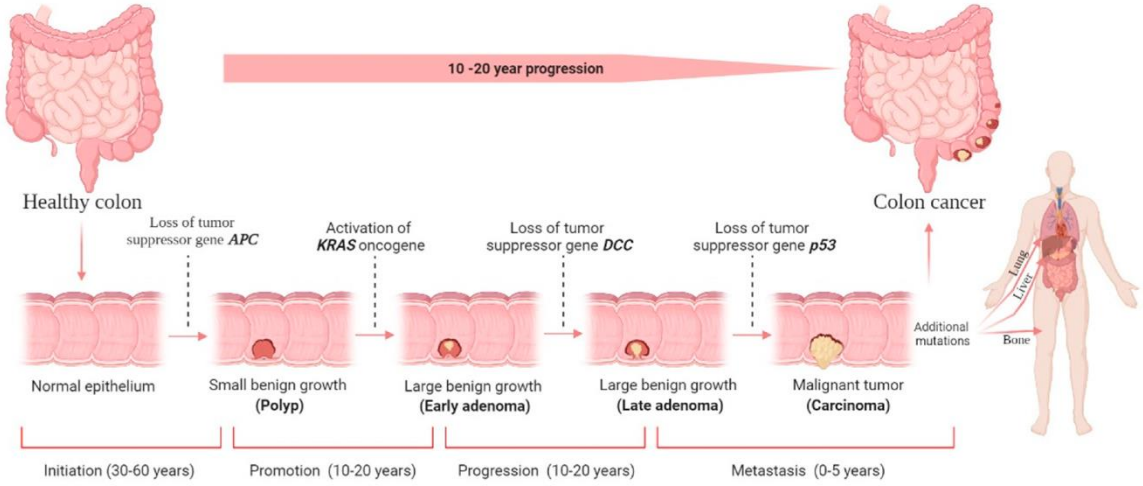

Figure 2-1. Colorectal cancer (CRC) stages and development. Taken from(Hossain et al., 2022).

Polyps are considered potentially dangerous to develop in various stages within the colon. In the early stages, small benign polyps form, typically causing no obvious symptoms, as shown in Figure 2-2. The risk of growing increases with age and is associated with factors such as a diet high in saturated fats, excessive sedentary behavior, tobacco or alcohol consumption, and chronic inflammatory bowel diseases (Hao et al., 2019; Øines et al., 2017). In the second stage, polyps may develop abnormal cellular changes, making them more likely to become cancerous. Complete removal of the polyps at this stage prevents cancer progression. In the third stage, the polyp may develop into carcinoma in situ, where cancerous cells are present in the polyp tissue but have not yet invaded the colon wall. In

the final stage, cancer becomes invasive and spreads through nearby tissues, lymph nodes, or other body parts.

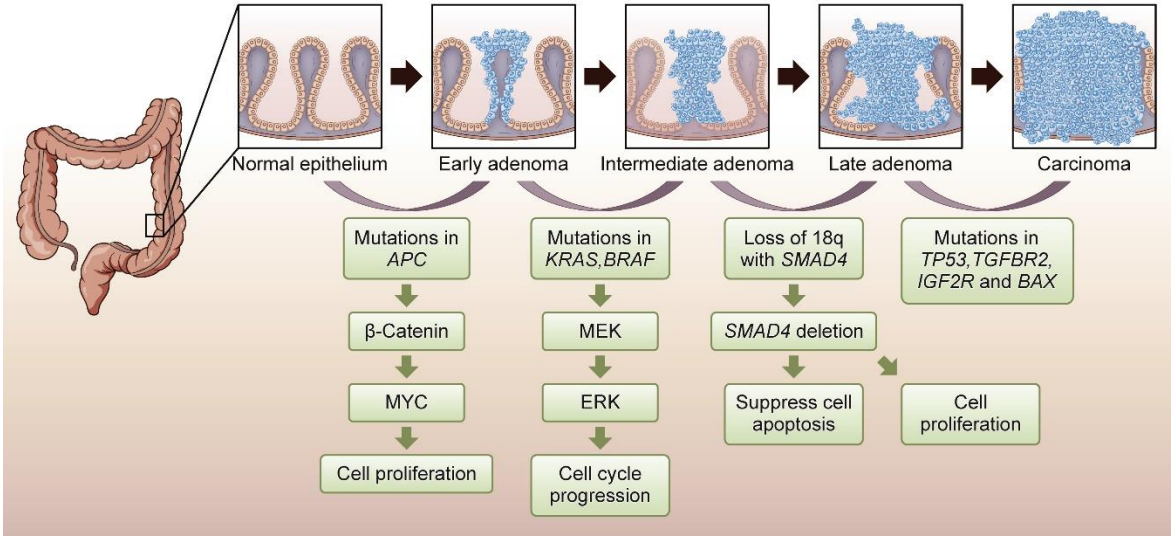

Figure 2-2. Tumor progression in colorectal cancer. Taken from (Luo et al., 2021).

Cancer manifestations depend on the individual's tolerance, the stage of the disease, and its location. In the early stages, patients may not experience apparent symptoms. However, as cancer grows and spreads in nearby tissues, intestinal habits become complicated, including persistent constipation, blood in the stool, severe abdominal pain, fatigue, weight loss, and others (Fritz et al., 2023; Holtedahl et al., 2021; Skalitzky et al., 2023). The etiology of this cancer is complex, involving both genetic and environmental factors. In the development of CRC, the APC, KRAS, and p53 genes mutate due to the accumulation of errors in DNA replication during cell division (Gavrić et al., 2024; Hasbullah & Musa, 2021). Mutations in the APC gene are observed early; this gene can deactivate its tumor-suppressing function, leading to uncontrolled cell growth and the formation of numerous polyps, even at a young age. The KRAS gene regulates cellular signaling during cell division, and mutations in this gene cause uncontrolled cell proliferation, which is associated with increased resistance to targeted treatments. Therefore, it is essential to determine the therapeutic approach for treating patients in the advanced stages of the disease. The p53 gene is a tumor suppressor gene responsible for DNA repair and inducing programmed cell death in damaged cells. Mutations in this gene deactivate its regulatory function, allowing abnormal cells to survive and multiply uncontrollably, increasing the risk of cancer development. Therefore, the detection of anti-p53 antibodies in blood serum indicates the presence of tumor cells expressing altered p53, making it a valuable biomarker for early detection of the disease (Iwamuro et al., 2015; S. Liu et al., 2020; Prats-Alfonso et al., 2012).

2.1.2 Biomarkers for Colorectal Cancer Detection

Biomarkers are observed as biological molecules that can be identified in samples such as blood, tissue, or stool. They provide valuable information about how the body responds to a disease. Their mere presence indicates the lack of self-regulation in the body and the level of risk a person may be exposed to. Biomarkers are categorized into several types: prognostic, genetic, predictive, pharmacodynamic, and recurrence (*Colorectal Cancer Biomarkers*, n.d.).

Prognostic biomarkers are used to estimate and identify the state and function of cells within the body. It helps estimate the most likely course of a disease in an individual and indicates the severity and risk of disease progression in the patient. Genetic-type biomarkers are based on genetic variations that influence susceptibility to diseases. They indicate the progression of disease and the effectiveness of medical interventions. Nucleic acid microarrays are a subject of study as they allow defining genetic markers in a sufficient sample size to predict the response of the most common cancers worldwide. Predictive biomarkers assess when treatment may or may not be effective in the body. Their utility is to predict the patient's response to treatment with a higher probability of success. Pharmacodynamic biomarkers play a role in measuring the effects of the dose administered in the body and evaluating the usefulness and efficacy of a treatment. Finally, recurrence biomarkers indicate when cancer appears again after treatment or if there is a risk of remaining cancerous cells.

Highlighting the importance of biomarkers in detecting biological changes associated with diseases, in the case of CCR, a variety of molecules lead to more accurate diagnoses, offering early intervention for the disease, as shown in Table 2-1.

Biomarker	Description	Function	Indication
Calprotectin (Ross et al., 2022)	A protein associated with intestinal inflammation; elevated levels in stool are indicative of gastrointestinal issues.	Serves as a marker to assess the level of inflammation in the intestines.	Inflammation resulting from conditions related to the presence of CCR.
CEA (Jeon et al., 2024)	Glycoprotein found in fecal tissue; after colorectal tumor resection surgery, elevated levels in the blood may indicate potential cancer recurrence.	Used for disease monitoring and assessing treatment effectiveness.	Indicator of tumor activity and recurrence.

p53 Gene (Michel et al., 2021)	Tumor suppressor gene: its mutation is directly linked to cancer as it disrupts the cell cycle, hinders apoptosis, and allows damaged cells to replicate and form tumors.	Used for detecting predisposition to cancer.	Directly associated with tumorigenesis (tumor formation).
KRAS and NRAS Genes (Bożyk et al., 2021)	This family of genes regulates intracellular signaling pathways involved in cell growth, differentiation, and survival. Mutations in these genes can lead to resistance to therapies targeting CRC. They are often associated with a poorer CRC prognosis, particularly in response to therapies like cetuximab and panitumumab.	Used to predict therapy response.	Influence therapy outcomes in CRC.
MicroRNA (miRNA) (Sur et al., 2022)	Plays a key role in regulating gene expression and can help predict the recurrence of CRC after initial treatment.	Used for early detection.	Indicates genetic changes associated with CRC.
DNA in Stool (Laugsand et al., 2020)	Fragments of mutated DNA associated with abnormal cells are released in the stool in the presence of CRC. These can be observed in precancerous lesions, such as adenomatous polyps. This method can be used to monitor	Non-invasive early detection.	Identifies genetic changes associated with CRC.

	treatment response and identify specific mutations, including those in the p53, APC, KRAS, NRAS genes, among others.		
C-Reactive Protein (CRP) (Thomsen et al., 2016)	A marker of systemic inflammation involved in the immune response to inflammation or infection. Cytokines are released, stimulating CRP production in the liver, which helps mark and eliminate invading pathogens.	Indicator of inflammation.	Inflammation is a contributing factor in some cases of CRC.
Interleukin-6 (IL-6) (Thomsen et al., 2016)	Molecule found in elevated serum levels are classified as pro-inflammatory cytokines, as they stimulate the production of cytokines that activate immune system cells. It is fascinating because it has been associated with resistance to apoptosis, promoting inflammation in the tumor microenvironment, and supporting the survival of abnormal cells.	Indicator of inflammation.	The link between inflammation and CRC.
Microsatellite Instability (MSI) (Gatalica et al., 2016)	Instability in microsatellites, which are repetitive DNA regions scattered throughout the genome, is associated	Used for detection and assessing recurrence risk.	A potential indicator of CRC recurrence.

	with a genetic predisposition to genomic instability, commonly observed in some CRCs.		
Anti-p53 antibodies (S. Liu et al., 2020; Suppiah & Greenman, 2013)	A tumor suppressor that regulates cell division and prevents the proliferation of cells with DNA damage, specifically in the presence of mutated or abnormal p53. It is present in a significant proportion of advanced colorectal tumors and can be detected in blood serum.	Indicates the presence of mutations in the p53 gene.	Potential biomarker for early detection and prognosis of CRC.

Table 2-1. Comparison of colorectal cancer biomarkers.

2.1.3 Detection and Diagnosis Methods of Colorectal Cancer (CRC)

Early detection of CRC is crucial in improving prognosis and treatment opportunities for patients. Although CRC impact is considerable due to its high morbidity rate, this type of cancer is highly treatable when diagnosed in its early stages. For this reason, the search for reliable and effective diagnostic methods remains a constant focus in the fight against this disease. In its early stages, CRC is practically undetectable as it lacks noticeable symptoms that indicate its presence, which varies depending on where the tumor is located and how it progresses in the tissue lining the colon or rectum (Marcuello et al., 2019; Vatandoost et al., 2016).

As mentioned earlier, colorectal tumors arise in different parts of the gastrointestinal tract. When the disease originates in the colon, it develops in a more significant portion of the large intestine, such as the cecum, ascending colon, transverse colon, descending colon, and sigmoid colon. When it originates in the rectum, it forms in the final part of the large intestine before the anal canal. Tumors originating in the colon are more challenging to detect in the early stages since the bleeding from the polyps mixes with the stool, making it more detectable immunologically through enzymes in the feces. On the other hand, when the primary tumor is in the rectum, it presents more noticeable bleeding and discomfort. The treatment of colon tumors involves surgical removal of the affected segment, while rectal tumors require more delicate handling due to their proximity to the anal sphincter. Treatment may include surgery, radiotherapy, chemotherapy, or anastomosis.

It is necessary to relate the patient's survival chances to the location of the primary tumor. A study by the National Cancer Institute (Kang et al., 2025) analyzed the effects, symptoms, and treatments of patients whose CRC originated in the left side of the colon (distal colon) and those whose cancer originated in the right side (proximal colon). The study, focused on 971 patients, supports the idea that cancers should be treated differently according to their origin. Some of the most common early detection tests in the clinical setting are:

Fecal Occult Blood Test (FOBT): When a patient experiences bleeding in the stool, it indicates the possible presence of precancerous polyps. As a non-invasive test, it involves an immunological or chemical study with an estimated 70-90% effectiveness in detecting cancer (Hewitson et al., 2007).

Colonoscopy: This is an invasive and therapeutic tool focused on introducing a flexible endoscope with a camera into the colon and rectum, allowing the doctor to visually examine the mucosa for polyps or tumors. This technique is one of the most effective, detecting up to 95% of CRC cases (Rex et al., 2015).

Sigmoidoscopy: This technique focuses on examining the lower part of the colon and the rectum rather than the entire colon. It involves an endoscope inserted into the distal colon and rectum. This procedure allows for the visualization of the mucosa and the detection of primary tumors in that region. Its effectiveness is 60-70%, but it significantly reduces its effectiveness by omitting observation of lesions in other areas of the colon (Schoen et al., 2012).

There are also imaging analysis techniques for CRC detection that are not as common due to infrastructure limitations but have a high detection rate for this disease. These methods offer varying degrees of invasiveness:

Computed Tomography Colonography (CTC): This technique uses computed tomography images to create a detailed view of the colon and rectum. These 3D reconstructions help detect polyps and masses in the intestinal lining. Its effectiveness is 90% in detecting polyps (Burling, 2010).

Magnetic Resonance Imaging (MRI): This technique uses magnetic fields and radio waves to form images of external tissues. The patient is placed in a scanner that generates a strong magnetic field, causing the atoms in the tissues to respond by emitting radiofrequency signals that generate 3D images, providing information on soft tissues. Its effectiveness ranges from 90% in detecting CRC, depending on the quality of the images formed. It is limited by time constraints compared to other techniques and the high equipment cost (Horvat et al., 2019).

Endorectal Ultrasound: This imaging reconstruction technique uses ultrasound waves to analyze areas surrounding the rectum. These waves bounce off the internal tissues and

convert the sound waves into images. High-resolution images achieve an effective rate of 90% (Edelman & Weiser, 2008).

2.2 Anti-p53 Antibodies as a Biomarker for CRC

2.2.1 Anti-p53 Immunology and its Relation to the p53 Gene

The immune system responds to foreign substances and abnormal components, such as abnormal cells produced in the body at a large scale. B and T lymphocytes are crucial in producing specific antibodies, known as immunoglobulins, as a defense mechanism against pathogens produced by cancerous cells. A series of changes in the protein pattern, called tumor stroma, occur, and the immune system seeks to recognize and neutralize abnormalities through a homeostasis process directed at tumor-related antigens.

The p53 gene encodes a crucial protein in regulating the cell cycle and preventing the proliferation of malignant cells. Its function is essential for safeguarding the integrity of the genome and maintaining cellular homeostasis. However, when tissues are exposed to carcinogenic agents capable of causing DNA damage, a process is triggered that can drastically alter cellular balance. Carcinogen exposure induces the formation of DNA lesions, known as DNA breaks, which disrupt the genetic sequence and may introduce mutations in critical genes, including the p53 gene. These mutations alter the functioning of the p53 protein and, consequently, disrupt its ability to regulate the cell cycle and prevent the development of malignant cells. The loss of its normal function can lead to a cascade of events that trigger cancer progression. Cells with mutations in the p53 gene may evade cellular control mechanisms, allowing for uncontrolled proliferation. Additionally, these cells with p53 anomalies can escape apoptosis, the programmed self-destruction mechanism of cells.

The alteration in the amino acid sequence of the resulting p53 protein due to mutations reduces its capacity to regulate gene transcription, which triggers an imbalance in gene expression. It contributes to tumor progression by activating cellular pathways, promoting survival and growth. These changes are associated with resistance to therapies and the ability of tumor cells to spread to other parts of the body, a process known as metastasis. The alteration of p53 function not only affects cell cycle stability and the prevention of malignant proliferation but also influences the ability of cells to respond to treatments such as chemotherapy and radiation therapy.

Antigen-presenting cells (APCs), macrophages, and dendritic cells detect and phagocytize tumor cells carrying the mutant protein through a major histocompatibility complex (MHC). For this process to occur, the antigens must be recognized by their primary structure (based on their amino acid sequence) by T cells, marking them for destruction by the target cells. In this case, a B lymphocyte-mediated response is not stimulated, as B cells typically

respond to the presence of foreign or bacterial antigens (Kang et al., 2025). The recognition of mutant p53 protein peptides by T lymphocytes triggers a specific immune response, initiating a series of events that release cytokines and perforins, amplifying other immune cells' activity and perforating the tumor cells' membranes in the CRC. As a result of this immune response, antibodies against p53 are generated by B cells in response to the presence of mutant proteins, becoming a diagnostic marker for CRC.

2.2.2 Characteristics of the Anti-p53 Antibodies as a Biomarker for CRC

The anti-p53 antibody is an immunoglobulin produced by the immune system in response to the presence of p53 antigens. It is selective towards the mutated or overexpressed protein in the body, meaning it avoids potential interference from other proteins present in the organism. As it is directly related to tumor suppression due to a mutation in the cell cycle and DNA damage, the mere presence of the antibody is a key indicator for detecting and diagnosing the presence of an abnormal tumor in the walls of the colon or rectum.

When the antibody encounters the mutated protein, an antibody-antigen-specific interaction occurs based on the complementarity of shapes and structures in the antibody's binding region (paratope) and the known antigen region (epitope). This reaction involves the non-covalent forces produced through van der Waals bonds. The following interactions explain the interaction of these bonds:

- **London Dispersion Force**: The non-polar regions in the three-dimensional structure of the p53 antigen establish interactions with the corresponding non-polar regions in the anti-p53 antibody. This process results in an intermolecular interaction that originates from temporary fluctuations in the electron distribution within the p53 protein. These fluctuations generate temporary dipoles that momentarily attract dipoles in the antiprotein, leading to London dispersion forces. Although these individual interactions are weak, their accumulation across the antigen-antibody binding interface leads to a stable complex.

- **Dipole-Dipole Interaction**: The p53 protein contains polar functional groups due to covalent bonds such as C=O (carbon-oxygen) and N-H (nitrogen-hydrogen) in specific amino acids. When these encounter the functional groups of the anti-protein, an electrostatic attraction occurs between the positive and negative dipoles of both molecules, contributing to the formation of a stable complex (forces associated with the molecules in the union).

- **Hydrogen Bond Interaction**: Both molecules' hydrogen and oxygen functional groups form hydrogen bonds. This biological interaction occurs when a hydrogen

atom covalently bonds to an electronegative atom (oxygen or nitrogen) to form an electrostatic interaction that results in a specific binding and molecular recognition.

2.2.3 Quantification of the Anti-p53 Antibodies and Its Clinical Importance

Evaluating anti-p53 antibodies in a biological sample provides crucial information that indicates the quantity of the antibody present throughout the disease, aiding in clinical decision-making. At the diagnostic level, detecting these antibodies is essential for the early identification of abnormal biomarker levels in the body, as their mere presence indicates the possible existence of an abnormal tumor in the gastrointestinal tissues. Generally, a higher concentration of antibodies may suggest a more advanced stage of cancer. However, the relationship between antibody levels varies according to the individual. Factors such as cancer aggressiveness, other conditions, and the patient's immune response may influence these levels.

The loss of immune tolerance caused by chronic inflammation in the disease state leads to the mass production of antibodies, which evaluates the response to treatment at any stage of CRC. In oncological treatment, monitoring anti-p53 antibody levels provides valuable information about the effectiveness of treatments such as surgery, chemotherapy, and targeted therapy, among others. A decrease in antibody levels could indicate a positive response to treatment, while remaining constant or increasing levels could signal treatment resistance. Relevant techniques for the immunological quantification of antitumor antibodies (AATs) include:

- **Multiplex ELISA for Specific Antibodies:** This technique uses microspheres or plates coated with the specific antibodies of interest. The biological sample extracted from blood serum is first treated with a blocker to prevent nonspecific binding with other proteins. The sample is then added to tubes or wells containing the coated microspheres or plates designed to capture the AATs in the sample selectively. The setup is sealed to prevent evaporation and incubation for 1 to 2 hours to allow the AATs to bind to the plate. The immunocomplex is then interacted with a reporter molecule. After incubation, washing removes unbound components and reduces background noise. The data is analyzed using specialized equipment and software, often spectrophotometry, to quantify each AAT's concentration.

- **Multiplex Flow Cytometry:** Begins with the isolation and washing of cell samples, followed by labeling antigens with specific antibodies containing fluorescent fluorochromes that emit light at different wavelengths. Chemical reactions ensure that fluorochromes bind to the antibodies without compromising their binding ability to target proteins. After a purification step to remove unused reagents, the effectiveness of the labeling is assessed by measuring the antibody-to-

fluorochrome ratio in a flow cytometer, enabling simultaneous detection and quantification of multiple proteins in a single cell.

- **Customized Protein Microarray Platforms:** Using specialized printing techniques, creating a microarray involves printing different proteins on a solid surface, such as glass slides or microarray chips. To facilitate binding, a functional layer is applied to the surface to optimize the protein-substrate interaction, and each spot on the array represents a unique protein. The target molecule from the sample interacts with the spots in the microarray. After labeling with a reporter and the washing steps, a reader can straightforwardly interrogate the target concentration. This meticulous approach creates a highly adaptable platform that enables the simultaneous analysis of multiple proteins in a single sample.

- **Next-Generation Sequencing (NGS) for Immunoglobulin Profiles:** NGS is a fundamental method for sequencing DNA and RNA in biological samples, where immunoglobulin-producing cells such as B and plasma cells play a critical role. Its relevance lies in the valuable information it provides about the immune response and the progression of CRC. The process begins with extracting nucleic acids from biological samples, followed by library preparation, which involves controlled fragmentation of DNA or RNA into ideal sizes for sequencing. Once prepared, these libraries undergo NGS technology, generating millions of short sequences in parallel. Fluorescent nucleotides are incorporated to read the sequence, and images are captured and translated into data. This data is analyzed bioinformatically to generate detailed immunoglobulin profiles, providing deep insight into the immune response and its evolution in the context of CRC.

2.2.4 Biosensor Devices in Biomarkers Detection

In the search for rapid detection methods that assist or complement medical decisions for the diagnosis and prognosis of cancer patients, sensitive, real-time detection and miniaturized technological devices are implemented. These devices rely on interactions between bioreceptors and the target analyte, while the sensing mechanism includes optical, electrochemical, piezoelectric, thermal principles, and electromagnetic waves. Biosensors utilize elements for molecular recognition, such as antibodies, nucleic acids, or aptamers, which specifically bind to their target analytes through highly selective interactions, such as antigen-antibody reactions, hydrogen bonding, or hybridization (Negahdary & Angnes, 2023; Pisoschi et al., 2024). The surface of transducers is modified with functional layers that allow specific binding with target biomolecules, ensuring selectivity, specificity, and sensitivity in detection. While specificity is the capability of target discrimination against one interferent at once, selectivity discriminates the target coexisting with multiple interferences in a complex matrix. Sensitivity refers to the slope of the calibration curve and is a function of analyte concentration or amount depending on the technology used and its application

areas. Detection of diseases by biosensor devices can also extend to environmental fields, such as pollutant detection and food safety, like pathogen detection.

A detailed classification of biosensors based on their transducer principles, including their working principle, main features, and representative examples in literature, is provided in Table 2-2.

Classification	Transducer	Working principle	Main features	References
Optical biosensors	Fluorescense	Uses the optical properties of matter to quantify and measure the properties of biological samples. The interaction of the sample with light of a specific wavelength induces fluorescence emission, which can be measured and quantified to obtain information about the molecules of interest.	Sensitivity – Fluorescence emission is highly sensitive to changes in molecular composition and can detect small amounts of molecules in a sample. Selectivity – It can detect fluorophores to specifically recognize and bind to the molecules of interest. Speed – It has the ability to measure fluorescent light emission in real-time.	Adeniyi et al., 2020; Lu et al., 2023; Reja et al., 2024; Singh et al., 2022
	Surface-Enhanced Raman Scattering (SERS)	Uses a rough metallic surface to amplify the Raman signal of molecules absorbed on it. The excitation of localized surface plasmons on the metallic surface is achieved through laser irradiation, enabling the detection of molecules at very low concentrations and their characterization using conventional Raman spectroscopy.	Sensitivity – The rough metallic surface enhances the Raman signal generated by the molecules of interest, allowing the detection of molecules at very low concentrations. Selectivity – Enables the specific detection and quantification of molecules that bind to the metallic surface. Versatility – This technique can detect a variety of molecules, including proteins, viruses, nucleic acids, and other compounds.	Kowalska et al., 2022; Zhou et al., 2023

			Multiplexing Capability – Allows the simultaneous detection of multiple molecules in a sample.	
	Photonic Crystals	Photonic crystals are modified with molecules that bind to the substance of interest. When the sample is applied to the surface of the crystal, a shift in the position of the photonic bandgap occurs, which can be used to quantify the amount of substance present in the sample. These crystals are used to detect biological molecules such as proteins, viruses, bacteria, and cancer cells.	Sensitivity – Achieved by measuring changes in the wavelength of light reflected by the crystal surface, enabling the detection of the molecule of interest at very low concentrations. Specificity – Achieved through the careful selection of materials used to fabricate the crystal, as well as the shape and arrangement of the components that make up its structure. Non-invasive – Does not require labels or markers that could damage the molecule of interest.	Bijalwan et al., 2021; Parandin et al., 2021
	Guided Mode Resonance (GMR)	This technique is based on detecting changes in the refractive index of a dielectric material using the resonance of light propagating along the interface between two materials with different refractive indices. Detection is achieved by monitoring changes in the angle or wavelength of light reflected at the interface, enabling the detection of molecules at very low concentrations.	Sensitivity – Measures the interaction of molecules on the biosensor's surface, producing a change in light reflection at a thin layer at the interface between the sample and the biosensor. It allows the detection of small variations in the molecular composition of the sample. Specificity – Designed to interact specifically with a molecule of interest. Speed – Enables real-time measurement of light reflection at the thin layer. Multiplexing Capability – This can be designed to detect	Yeh et al., 2021

			multiple molecules simultaneously.	
	Plasmons	These electron waves propagate on the surface of metallic materials, and their excitation by light causes changes in their reflection and absorption. In optical biosensors based on plasmons, these changes are used to detect the presence of biological molecules in a sample.	Sensitivity – Detects changes in the concentration of molecules near the biosensor's surface, producing a change in light reflection on the surface. Specificity – The receptor layer in the sensor is designed to interact with the molecule of interest selectively. Speed – Can provide real-time results.	Llamas-Garro et al., 2022; Mrozek et al., 2021
Electrochemical biosensors	Potentiometric	Measures the change in electrical potential generated by the interaction between an analyte and a bioreceptor attached to an electrode, correlated to the analyte concentration in the sample, allowing its quantification.	Sensitivity – Capable of detecting changes in electrical potential caused by the interaction of a molecule of interest with a biological recognition layer on the electrode surface. Specificity – Allows the specific detection of the molecule of interest using a specifically designed biological recognition layer. Stability – Can be used in a wide range of conditions, including pH, temperature, and salinity. Speed – Allows real-time detection of the electrical potential response.	Chen & Chou, 2011; Ivan et al., 2011
	Amperometric	Measures the electric current generated by applying a fixed potential. The electric current is produced from the analyte-bioreceptor interaction when a	Sensitivity – The electric current generated by the electrochemical reaction is proportional to the amount of analyte present in the sample.	

		mediator or the chemical reaction products are oxidized or reduced at the electrode surface. The magnitude of the current is analyte concentration-dependent, and the concentration of the analyte in the sample can be quantified by measuring this electric current.	Specificity – Use a selective electrode for the analyte of interest. Speed – Fast and allow real-time monitoring of the analyte concentration in the sample. Miniaturization – Can be miniaturized for use in portable or field applications.	Hou et al., 2020; Ortega et al., 2023; Vásquez et al., 2017
	Voltammetric	Measures the current when an analyte interacts with a bioreceptor attached to an electrode by applying a cyclic potential. A voltammogram can be generated by measuring the changes in electric currents as a function of the applied potential. The shape of the voltammogram is characteristic of the analyte in question, allowing for the identification and quantification of the analyte present in the sample.	Sensitivity – Can detect slight variations in the electric current produced by the electrochemical reaction. Highly sensitive and selective conductive materials, such as carbon nanomaterials and noble metals, can be used to improve sensitivity. Specificity – Selective coatings can be applied to the electrode to allow the specific binding of the molecule of interest. Speed – The voltammetry process is highly automated and can provide fast and accurate measurements quickly. Wide Detection Range – Can detect various compounds, from small molecules to macromolecules.	Eissa et al., 2021; J. Liu et al., 2022; Microchimica Acta 190 (4), 136
	Conductometric	Measures the electrical conductivity of a sample containing an analyte when interacts with a bioreceptor linked to a transducer. When the analyte binds to the	Sensitivity – Can detect minimal changes in electrical conductivity, allowing for detecting analytes at very low concentrations.	(Berketa et al., 2022; Soldatkina et al., 2018)

		bioreceptor, a change in the electrical conductivity of the sample occurs, either due to an increase or decrease in ion concentration, which is measured through an electrical circuit and related to the amount of analyte present in the sample.	Specificity – Achieved using specific recognition elements, such as antibodies, nucleic acids, or enzymes, designed to bind to the molecule of interest selectively. Speed – Enables real-time detection of the conductimetric response.	
	Impedimetric and capacitive	Measure the changes in impedance or capacitance at an electrode-electrolyte interface when the functionalized surface interacts with the sample containing the target analyte.	Sensitivity – It is extremely sensitive, i.e., It can detect concentrations of the target analyte in the order of fM and even lower. Specificity – Achieved modifying the transducer platform with specific biorecognition elements to bind specifically to the target molecule. Label-free – The ultrasensitivity makes amplification with labels unnecessary for quantification of extremely low concentrations of target analyte.	Biosensors and Bioelectronics 252, 116142; Sensors and Actuators B: Chemical 374, 132784; Talanta 243, 123337; Microchimica Acta 189 (6), 228
Piezoelectric biosensors	Piezoelectric Thin Film (PZT)	Uses a thin film of piezoelectric material, such as zinc oxide or lead titanate, coated with a bioreceptor to detect the interaction of a specific molecule. When the analyte binds to the bioreceptor, a change in the resonance frequency of the thin film occurs, which can be measured and correlated with the amount of analyte present in the sample.	Sensitivity – It can measure small amounts of mass on the sensor's surface through mechanical resonance, making it highly sensitive to detecting biomolecules. Specificity – This can be designed to be highly specific for certain molecules, enabling selective and quantitative detection of the molecule of interest.	(Kaur et al., 2023; Pohanka, 2017; Zhou et al., 2009)S

			Speed – The fast response of the piezoelectric thin film (PZT) to mass changes allows for real-time detection of biomolecules. Miniaturization Capability – Highly miniaturized and can be integrated into portable, low-cost devices.	

Table 2-2. Comparison and classification of biosensors.

3. Microwave Devices and Measurements

Microwave measurements rely on the interaction between electromagnetic waves and the sample under test (SUT). The primary property of interest is the complex permittivity (ε), which characterizes how a material interacts with electric fields at microwave frequencies. The complex permittivity is expressed as:

$$\varepsilon_r = \frac{\varepsilon' - j\varepsilon''}{\varepsilon_0} = \varepsilon_r^{'} - j\varepsilon_r^{''}, \tag{3-1}$$

where ε_r is the complex relative permittivity, and ε' and ε'' are the real and imaginary parts of the complex permittivity, respectively. The divisor ε_0 is the permittivity of free space ($\varepsilon_0 = 8.854 \times 10^{-12}$ F/m). Another important dielectric parameter is the dielectric loss tangent (Tan δ), which quantifies the ratio of the imaginary to the real part of the permittivity. It is defined as:

$$Tan\ \delta = \frac{\varepsilon_r^{''}}{\varepsilon_r^{'}} \tag{3-2}$$

This allows us to rewrite the expression for complex permittivity as:

$$\varepsilon_r = \varepsilon_r^{'}\ (1 - Tan\ \delta), \tag{3-3}$$

here, it is important to highlight that the dielectric loss tangent provides insight into the extent of energy dissipation within the material, where a higher loss tangent indicates greater energy absorption. In the context of biosensors using this technology, materials with an exceptionally low parameter are sought to guarantee that the dielectric substrate minimally absorbs the SUT.

A typical microwave measurement setup involves a Vector Network Analyzer (VNA), which measures the resonator's scattering parameters (S-parameters) with and without the SUT. The two key parameters measured are the reflection coefficient (S_{11}) and the transmission coefficient (S_{21}). These parameters provide insights into how the SUT affects the resonator's response. Such changes provide critical information about the dielectric properties of the material under test, facilitating accurate material characterization across various applications, including biomedical sensing and industrial monitoring.

The primary S-parameters of interest are the reflection and transmission coefficients, which are related to the intrinsic impedance of the material and the background medium (Balanis, 2005; Pozar & Schaubert, 2015). The reflection coefficient and transmission coefficient are expressed as:

$$S_{11} = \frac{V_1^-}{V_1^+}\Big|_{V_2^+=0} = \Gamma = \frac{Z_1 - Z_0}{Z_1 + Z_0} \tag{3-4}$$

$$S_{21} = \frac{V_2^-}{V_1^+}\Big|_{V_2^+=0} = T = 1 + \Gamma \quad (3\text{-}5)$$

where V_n^-, n = 1, 2, 3, …N, is the voltage reflected from port *n*, and V_n^+ represents the voltage incident on port *n*. In this context, the networks considered in this thesis are both reciprocal and symmetric, implying that $S_{11} = S_{22}$ and $S_{12} = S_{21}$.

3.1 Microwave Methods for Material Characterization

Microwave-based material characterization is widely used due to its ability to measure complex dielectric properties, such as permittivity and conductivity. These parameters provide essential information on how materials interact with electric fields at microwave frequencies, making this method valuable for applications ranging from biomedical, agriculture, geophysics, and energy industries (Hamdi et al., 2023; Kashyap & Kumar, 2021; Nasr & Sarabandi, 2024; Omam et al., 2022; Ramella et al., 2021; Saeidi et al., 2019; Vergnano et al., 2020). Several techniques are available for measuring dielectric properties using microwave technology (Ali Musa Mohammed, 2022; Mattsson, 2024); some of the most outstanding are the following:

Free space method

The free-space method is a non-contact and non-destructive technique used to characterize materials at microwave frequencies, particularly in high-temperature or harsh environments (Passos et al., 2024; Poyatos Martinez et al., 2021; Ramos et al., 2022). It utilizes two focused horn antennas aligned with the sample positioned between them. A VNA generates a microwave signal, transmitting it through one antenna and receiving it with the other. The interaction between the signal and the sample alters the transmitted and reflected signals, allowing the extraction of dielectric properties such as permittivity and permeability. A reference measurement, typically in the air, eliminates system losses and ensures accurate results.

The setup is depicted in Figure 3-1. This technique is ideal for large, irregularly shaped samples or materials that cannot be directly inserted into waveguides or coaxial probes. Post-processing techniques, like time-domain gating, filter out unwanted reflections from surrounding objects or sample holders, enhancing measurement accuracy. While calibration can be complex, the free-space method provides precise material characterization over a wide frequency range, making it valuable for aerospace, automotive, and materials research applications.

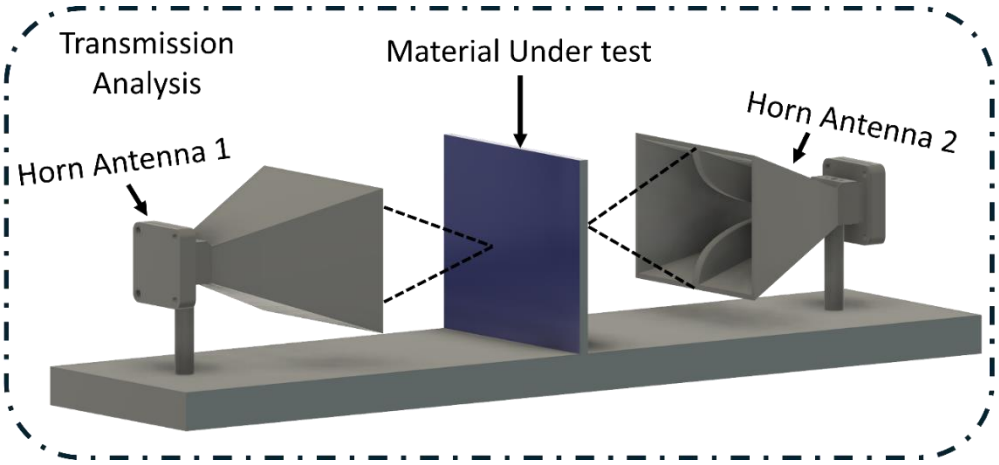

Figure 3-1. Schematic of the free-space measurement setup, featuring two horn antennas aligned with the sample under study positioned between them.

Open-Ended Coaxial Probe

The open-ended coaxial probe method is a versatile and non-destructive technique for characterizing the dielectric properties of liquids, semi-solids, and biological tissues (Joof et al., 2022; Vergnano et al., 2020). This method employs a coaxial probe with a cut-off end that is either pressed against the surface of a solid sample or immersed directly in a liquid. As microwaves propagate along the coaxial line, they generate fringing electric fields at the probe's tip, interacting with the sample. In this case, the VNA is used to measure the S_{11} parameter, from which the material's complex permittivity is obtained (Matković, 2024).

A schematic of the experimental setup is shown in Figure 3-2. This technique is highly sensitive and can measure small samples with minimal preparation. It is particularly suitable for analyzing homogeneous materials, biological tissues, and chemical solutions. Calibration is essential to ensure accuracy, typically involving reference liquids like distilled water, methanol, or saline solutions. Despite its simplicity and rapid measurement process, the technique requires careful handling to avoid air gaps or bubbles, affecting measurement precision. For this reason, it cannot be used with samples whose geometry is irregular. On the other hand, its portability and ability to perform in situ measurements make it valuable for medical diagnostics, food science, and chemical processing applications.

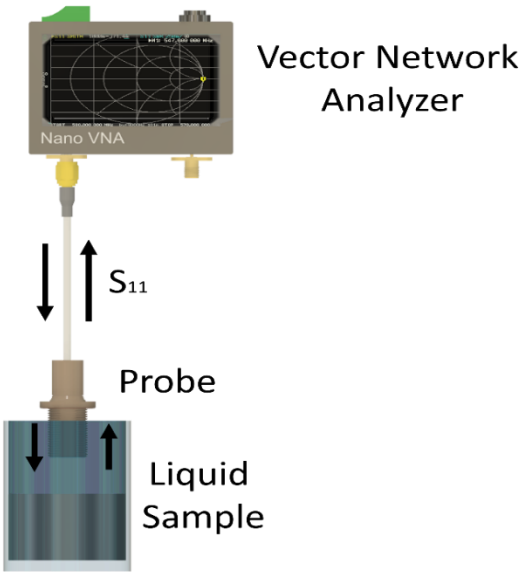

Figure 3-2. Schematic representation of the open-ended coaxial probe setup.

Transmission Line Method

The transmission line method involves placing the material under test inside a waveguide or coaxial transmission line, as illustrated in Figure 3-3. When the microwave signal propagates through the material, its interaction alters the propagation constant, affecting the measured scattering parameters (S_{11} and S_{21}). The dielectric properties are extracted by analyzing the phase shift and attenuation of the signal.

In this setup, the material is cut to fit precisely inside the waveguide or transmission line. A signal from the VNA is injected into the line, and the transmitted or reflected signal is recorded. The difference in the propagation constant between the empty and filled transmission lines is then used to calculate the permittivity through a calibration process. This method is well-suited for both solid and liquid samples, allowing for bulk property measurements over a wide frequency range. It is remarkably accurate for materials with moderate to high losses (Malkin et al., 2021; Raveendran & Raman, 2021; Stanley et al., 2023; Yang & Huang, 2021).

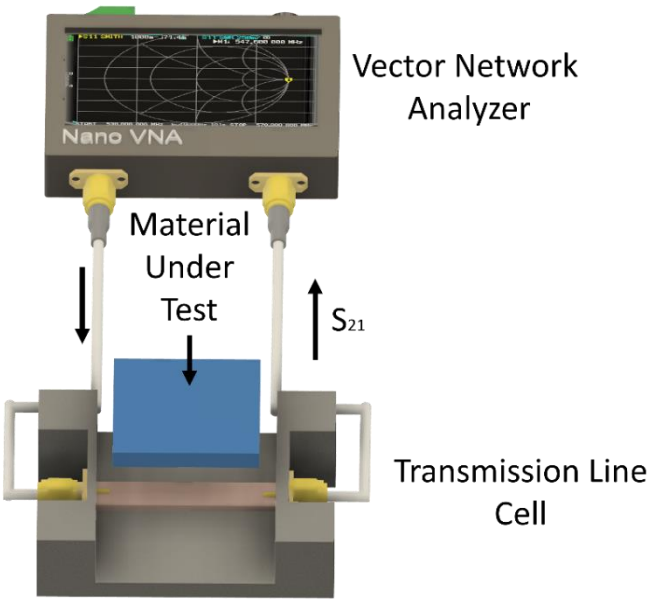

Figure 3-3. Schematic representation of the transmission line method setup.

Resonance-Based method

This method uses microwave cavities or microstrip resonators to characterize dielectric materials. The cavity's resonant frequency and quality factor (Q) are altered when a material is introduced into the resonator. The shift in frequency and Q-factor is used to calculate the sample's dielectric constant and loss tangent. The resonance-based method is illustrated in Figure 3-4, which shows the working principle of a resonator used to characterize dielectric materials (Almuhlafi et al., 2024; Tang et al., 2023).

The measurement setup starts with a resonator (cylindrical cavities, stepped ring resonators, or microstrip) designed to resonate at known frequencies. The sample is placed inside or near the resonator, and the VNA records the frequency shift. The change in resonance frequency (Δf_r) and the reduction in Q-factor indicates the dielectric constant and loss tangent. Advantages indicate extremely accurate for low-loss materials and high sensitivity to slight variations in dielectric properties requiring only small sample volumes (Bazgir & Sheikhi, 2024; Ma et al., 2021).

One of the primary advantages of this method is its extreme accuracy for low-loss materials. The resonance-based technique is susceptible to small variations in dielectric properties, making it ideal for detecting even subtle changes in the material's behavior. Additionally, it only requires small sample volumes, making it a more efficient choice when dealing with limited quantities of material or when high precision is required in measurements. The ability to achieve such accurate measurements without the need for large sample sizes is one of the key strengths of this technique.

Moreover, the resonance-based approach offers several advantages compared to other methods, such as the free-space method, the open-ended coaxial probe, or the transmission line method. While non-contact and suitable for large samples, the free-space method can be affected by environmental factors and requires careful calibration to eliminate system losses. The open-ended coaxial probe is limited in its application to homogeneous materials and liquids, and its sensitivity to irregular geometries can affect accuracy. On the other hand, the transmission line method requires precise sample dimensions to fit the waveguide or coaxial line, which may not be feasible with irregularly shaped or small samples (Alimenti et al., 2023). In contrast, the resonance-based method is less dependent on sample geometry and can achieve highly accurate and sensitive measurements with minimal sample preparation. It makes it particularly suitable for applications where small sample volumes are necessary, as the technique can detect subtle changes in dielectric properties without the need for large, uniform samples. Additionally, the resonance-based method excels in characterizing materials with low loss, which can be challenging to measure using other techniques.

The resonance-based method was chosen in this work based on the above. Moreover, the ability to perform measurements with small sample volumes is crucial to minimizing costs while ensuring reliable and reproducible results. This advantage makes the resonance-based approach a practical and efficient solution for biosensing applications, where sample availability may be limited, and precision is critical.

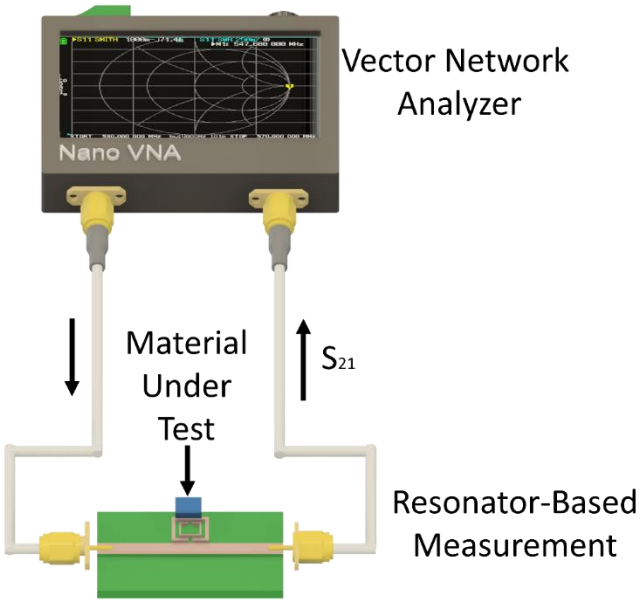

Figure 3-4. Schematic of the resonance-based method for characterizing dielectric materials using SSR microwave resonator.

3.1.1 Design Approaches for Microwave Transducers

The microwave-based transductor sensitivity depends on various factors that must be optimized during design. The performance of microwave sensors is critically dependent on their design, material selection, and optimization of resonator structures (Montoya-Villada et al., 2023; Morales-Guerra et al., 2021; Ossa-Molina et al., 2021; Reyes-Vera et al., 2024; Villada et al., 2023). Sensitivity, frequency stability, and quality factor (Q-factor) are key performance indicators that can be fine-tuned using electromagnetic simulation tools such as Computer Simulation Technology (CST) Studio and High-Frequency Structure Simulator (HFSS). These tools enable detailed modeling of the sensor geometry, material properties, and electromagnetic field interactions, allowing for iterative design improvements before fabrication.

Simulation is crucial in identifying potential weaknesses and enhancing transductor response, ensuring accuracy in real-world applications. The simulation process for microwave-based transducers involves multiple stages, each aimed at refining transducer performance and ensuring precision in material characterization. The first step involves creating a geometric model of the resonator using CAD tools integrated into CST or HFSS, allowing the user to manipulate dimensions and introduce design variations. Next, the dielectric substrate is selected based on its low-loss properties and high thermal stability to minimize signal attenuation and improve the transducer's Q-factor. The second step involves inputting the material properties of the transducer components (conductive materials, substrates, and the sample under test) into the simulation environment. The model is discretized into a mesh applied to regions of interest where electromagnetic fields are concentrated. A fine mesh accurately represents complex structures, particularly around resonators and coupling gaps, enhancing the precision of calculated scattering parameters (S-parameters). This stage is essential for capturing the subtle microwave-SUT interactions, directly influencing the transducer's sensitivity and performance.

In the third step, simulations are executed to analyze the reflection (S_{11}) and transmission (S_{21}) coefficients across the desired frequency range. The sample's dielectric properties can be extracted by examining the shifts in resonant frequency and amplitude variations. The results are iteratively analyzed, and adjustments to the transductor design, such as modifying resonator dimensions or coupling gaps, are made to enhance overall performance. Optimization techniques, including time-domain gating and frequency splitting, are applied to improve transducer sensitivity and reduce interference from environmental factors. The final stage tests the simulation results by comparing them with experimental data obtained from fabricated prototypes. Discrepancies between simulated and measured results are minimized through calibration processes and fine-tuning of the transducer geometry. This iterative workflow ensures that the microwave-based transducer meets performance expectations, achieving high sensitivity, stability, and accuracy in diverse applications such as biomedical diagnostics, material characterization, and environmental monitoring.

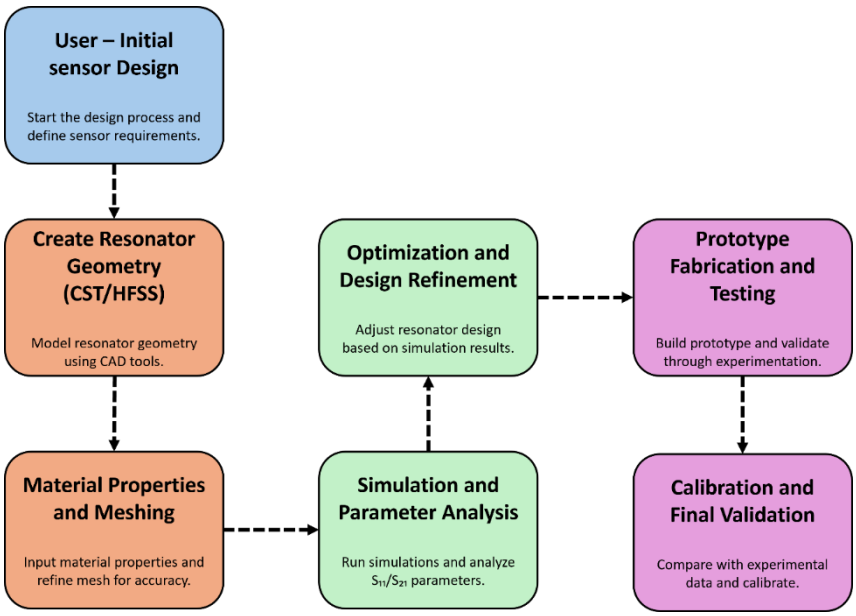

Figure 3-5. Flowchart of the microwave transducer design and optimization process.

3.2 Methods for Surface Biofunctionalization of Microwave-Based Transducers

Surface biofunctionalization is a critical process in biosensor fabrication, serving as a vital link between the bio and the transducer interfaces. This process enables the highly controlled attachment of specific biological molecules, such as proteins, nucleic acids, enzymes, and antibodies, to the solid surfaces of sensors (Gao et al., 2022; Kaymaz et al., 2023). Biofunctionalization methods establish a precise molecular connection between the biological components and the sensor's inert matrix. This bond is formed through chemical and physical interactions, creating a functional interface that allows for the highly selective and specific detection of target molecules. This molecular interaction directly affects the sensor's response, which is transduced into a measurable signal. The interpretation of this signal provides valuable information regarding the presence, concentration, and, in some cases, the activity of the target biological molecules.

This method involves introducing functional groups onto the surface, enabling the selective attachment of molecules and materials, thus opening a wide range of possibilities for creating materials with specific properties. In this process, chemical steps incorporate functional groups' reactive and specific atomic arrangements into the metallic surface. These functional groups act as anchors for the attachment of biological molecules, polymers, or other substances, allowing precise modulation of surface properties. Some of the most well-known techniques include:

Thermal evaporation

Thermal evaporation deposition involves heating a solid material until it reaches its evaporation point, transforming it into vapor. This vapor condenses on the surface at room temperature, creating a thin and uniform film. This technique is beneficial for depositing layers of organic or inorganic materials on solid substrates. The process is carried out in a vacuum chamber to ensure the absence of interference. However, this method is not suitable for directly functionalizing surfaces with biomolecules such as antibodies or ligands. Biomolecules are highly sensitive to high temperatures, and the conditions required for thermal evaporation would denature proteins, rendering them inactive.

A more accurate example of thermal evaporation applications would involve depositing metallic films that later undergo functionalization via alternative methods, such as chemical attachment or self-assembled monolayers, to immobilize biomolecules. For instance, metallic layers deposited by thermal evaporation can serve as the base for subsequent attachment of ligands (antibodies) through low-temperature chemical processes. For example, in detecting C-reactive protein in blood serum, the process begins with preparing the transductor surface and depositing a metallic layer using thermal evaporation. Subsequently, ligands (antibodies) are attached to the surface through chemical functionalization at low temperatures to preserve their activity. Figure 3-6 illustrates the steps involved in this process, including rinsing and blocking nonspecific bindings. Finally, the transducer response is analyzed to obtain valuable information about the presence of the target protein (Das et al., 2022; Garcia Alonso, 2012; Hsiao et al., 2024).

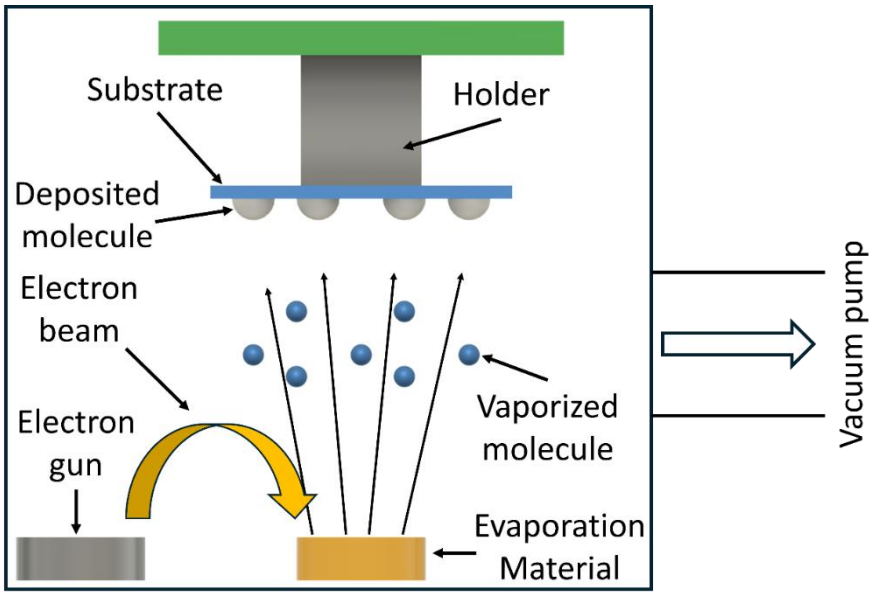

Figure 3-6. Schematic representation of the thermal evaporation process.

Silane Chemistry

Silane chemistry focuses on compounds that combine silicon and hydrogen atoms. Organosilanes, a class of these compounds, are used to establish covalent bonds between functional groups and the surface of a substrate. A practical example illustrating this technique involves the detection of PCR protein. Figure 3-7 shows the process begins with a meticulous surface cleaning. Next, a solution containing an organosilane compound with a specific functional group, such as thiol (-SH), is prepared. The surface is immersed in this solution and subjected to heat treatment to strengthen the disulfide bonds formed at a predefined temperature and duration. Once the surface is functionalized, the thiol groups react to form specific bonds between the protein and the surface, enabling detection through specialized techniques that analyze the response and provide valuable information on the protein-functionalized surface interaction (Hernandez et al., 2021; Mansur et al., 2009; Pasquardini et al., 2011; Puumala et al., 2022; Singh et al., 2022; Udomsom et al., 2021).

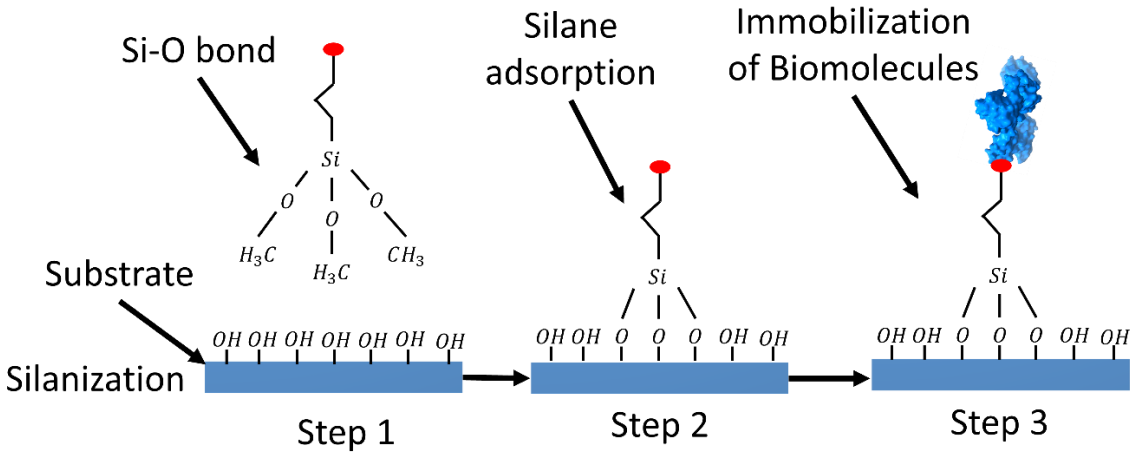

Figure 3-7. Schematic representation of the silanization process for biomolecule immobilization

Inkjet printing

Inkjet printing, widely known in the printing industry, finds a unique application in surface biofunctionalization. In this context, the ink droplets are not conventional but contain bifunctional ligands. An illustrative example is its use in creating DNA chips to analyze specific genetic sequences. The process begins with a solution of complementary DNA probes, which are converted into bifunctional ligands. Figure 3-8 shows that inkjet printing deposited microscopic probe patterns onto the chip surface, followed by a blocking step to prevent nonspecific binding. Once prepared, the DNA sample is introduced to the chip. Genetic sequences in the sample selectively bind to the printed probes at specific locations. Detection of these bindings is achieved through techniques such as fluorescence, enabling

highly selective and specific analysis of genetic sequences in a sample (Chatzipetrou & Zergioti, 2021; Hussain et al., 2022; Trotter et al., 2020; Zub et al., 2022).

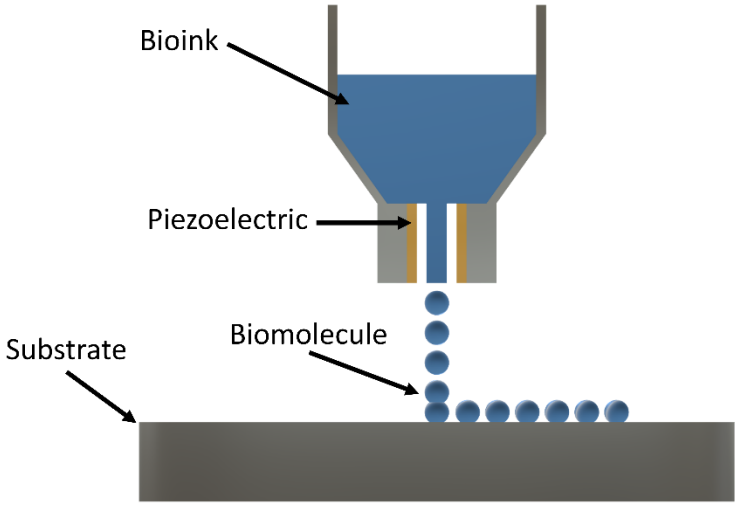

Figure 3-8. Schematic representation of inkjet printing for surface.

Self-assembled monolayers

The formation of self-assembled monolayers (SAM) (Figure 3-9) is a technique in which a solution of organic molecules with a functional group at one end (anchor group) chemisorb onto a metallic surface (Frasconi et al., 2010; Lundin et al., 2022), followed by interaction with a functional ligand or receptor molecule, through, i.e., hydrogen bonds or van der Waals forces, etc. For example, when depositing a thiolated SAM (carboxylated at the other end) at a gold layer, the steps include preparing the gold surface to remove impurities, immersing the surface in the solution containing the molecules to form the SAM, and rinsing the surface to eliminate excess unbound molecules. Subsequently, a second functional ligand containing amino groups from a protein or antibody may be linked, for example, through carbodiimide crosslinking chemistry. The thiol molecule can also end with a maleimide functional group, which has an affinity for thiol groups, forming a second functional layer. An enzyme modified with thiol groups can then be placed on the functionalized surface. The interaction between maleimide and thiol groups forms a robust covalent bond, ensuring the stable attachment of the enzyme to the surface. Thiol moieties can also be at each end of the SAM-forming molecule to link, for example, with metallic labels. The surface is rinsed again to remove excess molecules, and it is then used for the specific detection of substrates in biosensing applications (Houseman et al., 2002).

The choice of using SAM chemisorbed over copper-based microstrip transducers in this thesis is driven by the simplicity and efficiency of the SAM technique. SAMs allow direct functionalizing of a metallic surface with organic molecules that bind specific biomolecules via interactions, such as hydrogen bonds or Van der Waals forces, without complex

fabrication steps. Likewise, the SAM technique enables a straightforward approach to functionalizing the sensor surface, providing high specificity for biomolecule detection with minimal sample volume and preparation. Finally, SAMs offer a high degree of stability and are easier to scale for biosensing applications, mainly when dealing with limited sample quantities or when cost is a primary concern.

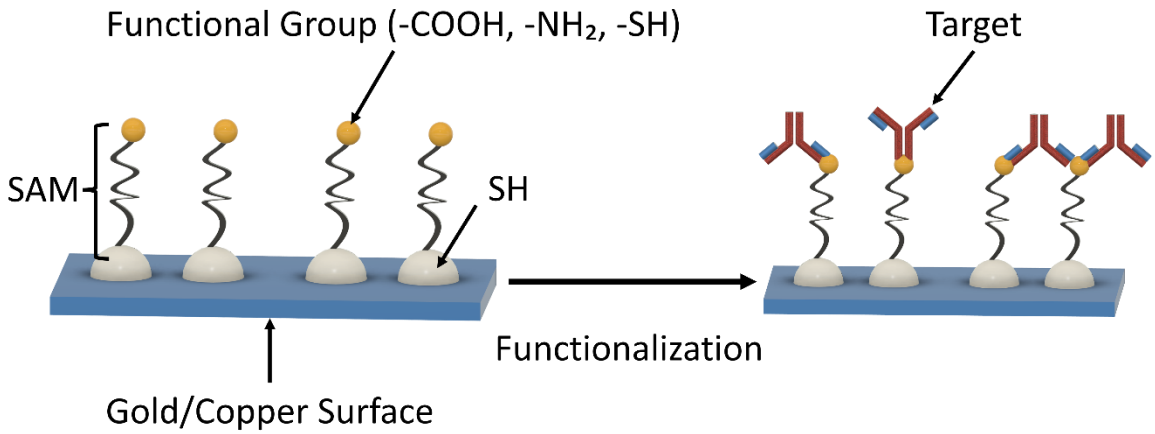

Figure 3-9. Schematic representation of a self-assembled monolayer on a substrate.

4. Sensor Development in the Microwave Region

4.1 Operating Principle

This thesis proposes a microwave-based transducer incorporating stepped impedance resonators (SIRs) into a microstrip line. This arrangement aims to identify slight changes in the dielectric characteristics of an SUT by monitoring alterations in the biosensor's resonance frequency. The operational concept includes the relationship between the biosensor's electromagnetic fields and the surrounding medium's dielectric characteristics. Any alteration in the dielectric permittivity of the SUT leads to a quantifiable shift in the transducer's resonance frequency, directly indicating the SUT's characteristics (Naqui et al., 2016; Su et al., 2016).

An innovative aspect of this biosensor is its transducer, based on a microstrip line configured with two identical SIRs connected in a shunt configuration. This setup offers several advantages, such as increased sensitivity to changes in dielectric properties and improved immunity to external interferences like temperature and humidity fluctuations. These environmental factors can vary frequently in real-world settings, leading to measurement errors. By employing a differential configuration, the responses of the two resonators can be directly compared, enhancing transducer accuracy and facilitating the detection of minimal dielectric perturbations.

Mathematically, the resonance frequency f_r of an SIR resonator is determined by the following equation:

$$f_r = \frac{1}{2\pi\sqrt{L_s(C_s \pm |\Delta C_s|)}} \tag{4-1}$$

In this expression, Ls represents the inductance of the resonator, while Cs denotes its nominal capacitance. The term ΔC_s corresponds to the capacitive perturbation induced by the presence of biomolecules or changes in the dielectric permittivity of the medium. Any modification in ΔC_s generates a measurable shift in the resonance frequency, directly indicating the detected disturbance. Thus, the resonance frequency shifts upward or downward depending on the magnitude and nature of the dielectric disturbance. This shift determines the SUT's dielectric constant and loss tangent.

The relationship between the perturbation and the resonance frequency can be expressed as:

$$f_0 = \frac{1}{2\pi\sqrt{(L_s - |M|)(C_s \pm |\Delta C_s|)}} \tag{4-2}$$

where *M* represents the mutual inductance between the resonators. The coupling between the resonators is essential for improving sensitivity and discrimination in detecting dielectric changes (Acevedo-Osorio et al., 2020; Boruah et al., 2021). The proposed transducer uses a differential configuration consisting of two identical SIRs placed on opposite sides of the microstrip line. This arrangement allows for a more robust sensing mechanism, minimizing the impact of external environmental factors such as temperature and humidity. The differential setup operates by comparing the dielectric properties of two samples: a reference and the SUT. The difference in their dielectric permittivities causes a split in the resonance frequencies, enabling precise detection of slight variations (Naqui et al., 2016; Su et al., 2016). On the other hand, a magnetic coupling between the resonators plays a crucial role in this design, as it generates a split in the resonance frequency when a dielectric disturbance is introduced in one of the resonators. For this configuration, the magnetic coupling coefficient k_m is expressed by the following expression:

$$k_m = \frac{-|M|}{L_s} \tag{4-3}$$

This coefficient reflects the strength of the mutual inductance between the resonators. Magnetic coupling introduces two distinct resonance frequencies, f_{r1} and f_{r2}, depending on the dielectric perturbation in each resonator. The difference between these frequencies provides the differential output that characterizes the SUT.

4.2 Equivalent Circuit Model

Figure 4-1a shows the equivalent circuit model of the sensor, representing the electrical elements that describe the electromagnetic behavior of the system. The SIR resonators are modeled using capacitors (C_s) and inductors (L_s), which represent their capacity to store electric and magnetic energy, respectively. Variations in capacitance (ΔC_{s1} and ΔC_{s2}) are used to model the effects of geometric changes or dielectric perturbations in each SIR. Additionally, the magnetic coupling between the resonators is represented by *M*, which directly influences the resonance frequencies, the separation between peaks, and the sensor's bandwidth.

The model includes a central line with a characteristic impedance of 50 Ω, divided into two sections to represent the contribution of the main transmission line. A global capacitor (*C*) is incorporated to model the system's total capacitance, affecting the frequency response and allowing fine-tuning of the resonance. As explained above, the magnetic coupling coefficient (km), which quantifies the electromagnetic interaction between the resonators, is calculated using equation 4-3.

In addition, if the capacitive perturbations are identical ($\Delta C_{s1} = \Delta C_{s2}$), the sensor is balanced (i.e., identical perturbations), according to the circuit of Fig. 4-1a, it can be readily noticed

that the structure exhibits a single zero transmission, which can easily be determined using equation 4-2. In the presence of coupling, the zero transmission shifts upward. The resonance frequency in this equation is denoted by f_0.

On the other hand, the splitting of the resonance frequencies due to coupling can be described using the following expressions for f_{r1} and f_{r2}:

$$f_{r1,r2} = 2\pi\sqrt{\frac{L_s(C_{s1}+C_{s2}) \pm \sqrt{[L_s(C_{s1}-C_{s2})]^2+4C_{s1}C_{s2}M^2}}{2C_{s1}C_{s2}(L_s^2-M^2)}} \quad (4\text{-}4)$$

These expressions provide a mathematical framework to understand how the sensor's resonance frequencies shift when a dielectric perturbation occurs in one of the resonators. The presence of two distinct resonance peaks enables the sensor to perform differential measurements, where the separation between the upper and lower frequencies directly indicates the dielectric contrast in the SUT. This capability is particularly useful for detecting subtle changes in the dielectric properties of biological samples or other materials with varying permittivity.

4.3 Design of the Microwave Transducer Region

The transducer design was optimized through an electromagnetic simulation using CST Studio 2024, aiming to operate at a frequency close to 5 GHz. These simulations allowed for the analysis of electromagnetic field behavior, fine-tuning of geometric parameters, and optimization of sensor sensitivity while minimizing measurement losses. Figure 4-1b depicts a schematic of the proposed transducer. The substrate used in the transducer's fabrication is a Rogers RT 6002 dielectric sheet with a width (*W*) and length (*L*) of 20 mm each. This material has a relative permittivity of ε_r=2.94 and a low loss tangent (*Tan δ*) of 0.0012.

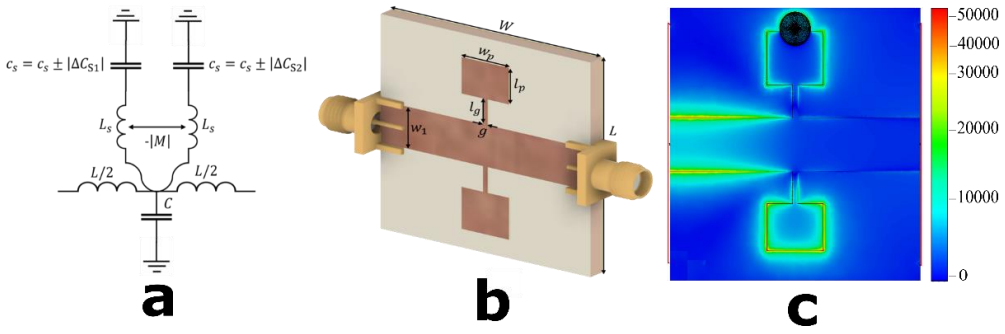

Figure 4-1. Design of the microwave-based transducer region. a) Equivalent circuit diagram of the stepped impedance resonator (SIR). b) Schematic of the copper transducer built from a microstrip line section loaded with a pair of SIRs. c) Simulated electric field distribution in the microwave transducer at 5 GHz. The color scale represents the magnitude of the electric field intensity in V/m.

From a geometric perspective, the microstrip line has a width (w_1) of 3.9 mm, designed to ensure a characteristic impedance of 50 Ω. It is connected to two capacitive SIR structures. The capacitive nature of the SIR structures allows them to store and concentrate the electric field, thereby enhancing sensitivity to any sample placed near them. Each capacitive structure has a width (w_p) of 4.5 mm and a length (l_p) of 3.9 mm. The microstrip lines connecting the main microstrip line to the SIRs measure 2.4 mm in length (l_g) and 0.43 mm in width (g), defining the electromagnetic coupling between these elements and ensuring efficient energy transfer to the resonators. The dimensions of these structures were optimized to minimize energy coupling between the two resonators.

The simulation results shown in Figure 4-1c reveal a non-uniform distribution of the electric field intensity within SIR structure. Notably, the highest intensity is observed at the upper edges of the SIR, forming localized regions of strong electric field confinement. This electric field concentration is critical for the sensor's sensitivity to dielectric perturbations. Any change in the dielectric properties of the material in proximity to these regions, such as a variation in permittivity or conductivity, will directly influence the electric field distribution. It leads to a quantifiable alteration in the resonance frequency of the SIRs, offering a precise method for detecting and measuring dielectric changes.

The geometric dimensions of the capacitive structure were enhanced by parametric analysis. This parametric analysis systematically assessed the influence of the large gap (l_g) and width gap (g) on the sensor's resonance behavior. Figure 4-2a illustrates how increasing l_g from 2.15 to 3.4 mm causes a gradual decrease in the resonance frequency, with shifts of approximately 245 MHz for every 0.25 mm increment. This behavior is attributed to the increased coupling length, which enhances energy transfer between the resonators. However, while larger values of l_g improve coupling; they also result in broader resonance peaks, which reduce the sensor's resolution. Broader peaks make it more challenging to distinguish small dielectric changes, thereby affecting the sensor's accuracy in material characterization. Similarly, the effect of g on the sensor's performance is shown in Figure 4-2b. Reducing the gap from 0.53 to 0.23 mm increased the coupling strength, sharpening the resonance peaks and improving the sensor's resolution. However, gaps smaller than 0.28 mm pose practical challenges in fabrication due to tooling limitations and machining tolerances in CNC milling. Achieving consistent and reliable fabrication of such small gaps can be difficult, increasing the risk of defects that could negatively impact the sensor's performance. Based on these results, the optimal values of l_g= 2.4 mm and g = 0.43 provided the best trade-off, achieving sharp resonance peaks with high sensitivity and stable performance, ensuring reliable detection of small changes in material properties.

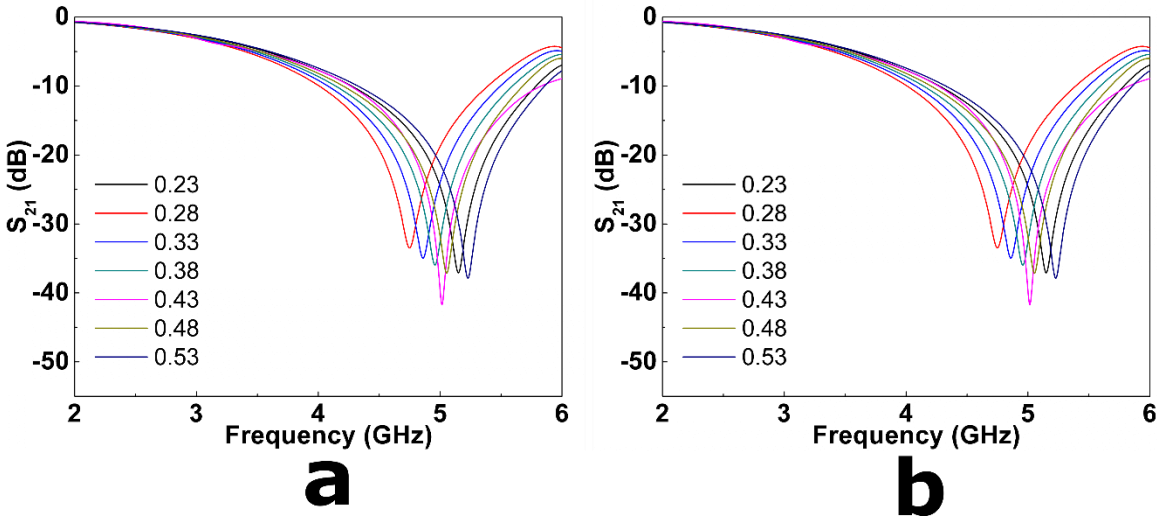

Figure 4-2. Simulated S_{21} parameter response of the SIR resonator for varying dimensions a) large gap ($\boldsymbol{l_g}$) and b) width gap ($\boldsymbol{g}$) in mm. These variations maintained the following dimensions constantly: $\boldsymbol{W}$, $\boldsymbol{L}$, w_1, w_p, l_p.

4.4 Transducer Fabrication

The proposed microwave-based transducer was fabricated using a high-precision CNC milling machine (LPKF ProtoMat D104, LPKF Laser & Electronics AG, Hanover, Germany). This method was selected to ensure accurate engraving of the critical components, such as the upper transmission line, stepped impedance resonators, and specified gaps, with micro-level precision. As mentioned in section 4.3, the transducer was fabricated on a Rogers RT 6002 substrate chosen for its excellent dielectric properties and low moisture absorption. The top copper layer, with a thickness of 35 µm, was etched to form the microstrip line and the SIRs, while the bottom layer remained a continuous copper film to serve as the ground plane.

Following the milling process, the ends of the 50-Ω microstrip line were soldered to 50-Ω SMA male connectors (SOUTHWEST 292-07A-5, Southwest Microwave, Tempe, AZ, USA) to facilitate efficient signal transmission and precise measurement of the transmission coefficient. The integration of these connectors ensures proper impedance matching with the measurement devices, reducing reflection losses and optimizing the microwave transducer's performance during experimental testing.

4.5 Experimental Validation of the Proposed Transducer

Once the transducer was fabricated, its experimental response was systematically evaluated. The initial step involved testing the transducer's response without a SUT. This baseline measurement aimed to compare its experimental performance with simulation results and establish its operational resonance frequency. The process begins with calibrating the VNA (FSH8, Rohde & Schwarz, Munich, Germany) to eliminate systematic errors and ensure high measurement accuracy. The VNA was configured in high-precision mode and calibrated over a 2 to 6 GHz frequency range using the impedance calibration kit (FSH-Z28, Rohde & Schwarz, Munich, Germany). The calibration followed the standard open-short-load-through (OSLT) procedure involving compensating for different factors. The open circuit calibration addresses parasitic capacitances; the short circuit calibration corrects parasitic inductances; the load calibration ensures proper impedance matching, and the through calibration accounts for insertion losses along the transmission path between the ports. After the calibration, the SUT is placed on the sensitive area of the resonator, and the S_{21} parameter is recorded over the specified frequency range.

Figure 4-3a illustrates that the experimental responses of the proposed microwave-based transducer without SUT show a slight resonance shift compared to the simulated response. Although the transducer was initially designed to operate at 5 GHz based on simulations, the experimental results revealed a resonance frequency of 5.2 GHz. This deviation of 200 MHz, equivalent to an error of approximately 4%, falls within acceptable limits for practical microwave transductor implementations. This small difference between experimental and simulated results can be attributed to manufacturing tolerances and slight variations in material properties. Next, a controlled experiment using a water droplet as the test medium evaluated the sensor's behavior under SUT interaction. A droplet of precisely 5 µL deionized water was carefully placed on the capacitive region of the sensor’s surface. Deionized water was chosen for its well-characterized dielectric properties, with a relative permittivity of approximately 80.

Simulations were performed to predict the transducer’s response under these conditions, estimating a primary resonance shift to 4.84 GHz. The transducer demonstrated a resonance frequency of 4.97 GHz, resulting in a shift of 229 MHz from the dry experimental baseline of 5.2 GHz. The calculated error for this primary resonance shift is approximately 2.54%, which is within acceptable limits for experimental setups involving liquid interactions. The observed leftward shift in resonance frequency is consistent with an increase in the effective permittivity of the surrounding medium, a direct consequence of water's high dielectric constant. The increased effective capacitance of the resonator reduced its natural oscillation frequency.

Additionally, the presence of the water droplet introduced a second resonance peak due to the broken symmetry between the two resonator structures. This phenomenon occurs because introducing the water droplet creates an asymmetry in the electric field distribution, resulting in separate resonances for each resonator. In simulations, this second resonance appeared at 3.92 GHz, while experimentally, it was observed at 3.8 GHz, corresponding to a deviation of 120 MHz and an error of approximately 3.06%. The analysis of these results demonstrates that the transducer can detect changes in the surrounding medium with high accuracy while introducing a second resonance peak, which provides additional information about the system's behavior. This feature enhances the transducer's sensitivity and provides a robust mechanism for distinguishing different dielectric properties of the SUT.

The final step of the experimental validation involved assessing the transducer's ability to detect changes in dielectric permittivity by analyzing glycerin-water mixtures with varying glycerin concentrations. Glycerin and water were chosen for this experiment due to their well-documented dielectric properties, which provide a controlled range of permittivity values. Glycerin has a dielectric constant of approximately 47, while water exhibits a significantly higher dielectric constant of about 80. By preparing mixtures with glycerin concentrations of 0, 20, 40, 60, 80, and 100% by volume (glycerin dissolved in water), a systematic evaluation of the transducer's sensitivity to dielectric variations was conducted.

Each mixture was carefully applied to the transducer's surface in a controlled volume of 5 µL, targeting the area with the highest electric field intensity as identified in the design simulations. The application of a consistent droplet volume ensured uniform measurement conditions across all samples, minimizing variability due to sample handling. The controlled placement of the droplet on the capacitive region of the transducer enabled effective interaction with the resonator's electric field, facilitating accurate detection of dielectric changes.

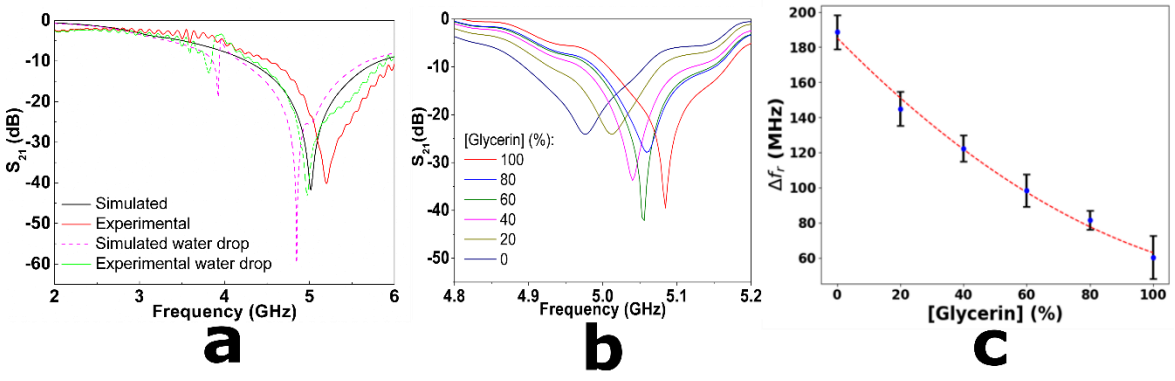

Figure 4-3. a) Simulated and experimental S_{21} transducer responses under dry conditions and with a 5 µL water drop. b) Measured S_{21} parameter response of the sensor for varying concentrations of glycerin-water mixtures. The resonance frequency shifts progressively towards higher values as the glycerin concentration increases. c) The calibration curve shows the relationship between the resonance frequency shift ($\boldsymbol{\Delta f_r}$) and the concentration of glycerin-water mixtures. The red dashed line represents the quadratic fit to the experimental data.

Figure 4-3b illustrates the spectral responses of the transducer for all glycerin-water mixtures, highlighting the progressive shifts in resonance peaks as the glycerin concentration increases. The spectral data reveal a clear trend: at 0% glycerin (pure water), the resonance frequency at 4.97 GHz was observed. As the glycerin concentration increased, the resonance frequency shifted rightward, reaching 5.01, 5.04, 5.05, 5.06, and 5.08 GHz at 20, 40, 60, 80, and 100% glycerin, respectively. The total difference in resonance frequency between 0 and 100% glycerin is 104 MHz, showcasing the sensor's sensitivity to the changes in the medium's dielectric properties caused by the transition from water to glycerin. The experiment was repeated three times for each glycerin-water concentration to ensure accuracy and repeatability in constructing the calibration curve shown in Figure 4-3c.

The calibration curve is described by the quadratic equation 4-1:

$$\Delta f_r = 0.006x^2 - 1.829x + 185.252 \quad (4\text{-}5)$$

Where x represents the extent of glycerin in the water solution. The quadratic regression coefficient $R^2 = 0.993$ indicates an excellent correlation between the quadratic model and the experimental data, demonstrating the sensor's accuracy in detecting dielectric changes.

5. Biosensor Functionalization

The biofunctionalization process of the microwave-based transducer is essential to provide it with the specificity and selectivity required for detecting anti-p53 antibodies. This procedure involves optimizing the transducer's sensitivity, minimizing nonspecific interactions, and enhancing its performance in complex biological environments. This process begins with coating the transducer surface with a SAM of 3,3′-Dithiodipropionic acid di(N-hydroxysuccinimide ester) (DTSP). This monolayer acts as an intermediary linker that facilitates the covalent immobilization of the p53 protein, ensuring an orderly and stable arrangement on the biosensor surface. The presence of p53 on the functionalized surface enables highly specific detection of anti-p53 antibodies, which is crucial in diagnosing certain pathologies such as CRC.

During the study, immobilization concentrations and times were optimized to maximize the specific binding of p53 protein and antibodies interaction and reduce unspecific interactions with other biomolecules present in complex samples, such as blood serum. This control is essential to minimize noise in the measurements and maintain the biosensor's accuracy. A blocking strategy using BSA was also implemented to cover unoccupied sites on the biosensor surface. This technique prevents nonspecific interactions and enhances the selectivity of the device, ensuring reproducible and reliable results during the detection process. Combining these steps ensures that the biosensor operates with high sensitivity and specificity, even in complex biological matrices.

5.1 Materials

p53 Protein Linking and Non-Specific Interactions Blocking

The p53 protein was selected as the recognition molecule due to its ability to specifically interact with anti-p53 antibodies, the target analyte of the biosensor. This interaction ensures that shifts in resonance frequency (Δf_r) exclusively reflect the specific protein-antibody binding, guaranteeing measurement accuracy. Different concentrations (1.0, 2.5, 5.0, 10.0, and 20.0 µg/mL) and incubation times (1, 2 h, and overnight) were evaluated to optimize the immobilization of p53 on the biosensor surface without compromising its functional activity. These conditions were optimized to maximize immobilization efficiency and improve the stability of biomolecular interaction.

Bovine Serum Albumin (BSA) was used as a blocking agent to cover nonspecific binding sites on the sensor surface, thereby reducing nonspecific interactions from interfering molecules. 0.1, 0.5, and 1.0% BSA were evaluated, with an incubation time of 2 h, sufficient to stabilize the biosensor's response.

Anti-p53 Antibody

The anti-p53 antibody, the specific analyte of the biosensor, is crucial in the early detection of CRC owing to its strong correlation with p53 protein mutations. These mutations manifest in the initial phases of disease progression, rendering anti-p53 antibodies a viable biomarker for the early diagnosis of this cancer type. This study evaluated antibody concentrations (0.0, 250.0, 500.0, 750.0, 1000.0, and 1250.0 pg/mL) to characterize the biosensor's response. These measures helped establish the device's linear dynamic range and sensitivity, ensuring a direct and proportional correlation between anti-p53 antibody concentrations and shifts in resonance frequency (Δf_r). Additionally, incubation times (30, 45, and 60 min) were optimized to ensure efficient interaction between the antibody and the functionalized biosensor surface.

5.2 Biosensor Preparation and Functionalization Protocol

The preparation and functionalization of the microwave-based biosensor follow a detailed procedure, as described below and illustrated in Figure 5-1. In the first step **(I)**, the sensor surface is prepared through mechanical polishing using a metallographic grinding and polishing machine (Metapol 160E, Laizhou Lyric Testing Equipment Co., Ltd, Shandong, China). Alumina suspensions with particle sizes of 0.30 and 0.05 µm are used for 20 min each. This process removes surface irregularities and contaminants, ensuring a smooth and uniform surface essential for forming SAMs. The surface is then cleaned by ultrasonic treatment in acetone for 7 min, followed by rinsing with distilled water, leaving the surface free of residual particles and organic contaminants.

The second step **(II)** involves the chemical etching of the copper surface to expose fresh atoms and enhance the availability of reactive sites. A 5 µL drop of 32.5% HNO_3 is applied for 1 min, followed by a 5 µL drop of 3.7% HCl for 6 min. This pre-treatment removes oxide layers and any remaining impurities. The surface is subsequently rinsed with distilled water and subjected to ultrasonic treatment in a distilled water bath for 7 min to eliminate any acidic residue. This process ensures a highly reactive surface for the formation of dense and uniform SAMs.

In the third step **(III)**, a SAM of DTSP is formed on the transducer surface. A DTSP solution at a concentration of 4 mM in dimethyl sulfoxide (DMSO) is prepared and directly deposited by casting a 5 µL volume onto the activated surface. The sensor is incubated at room temperature for 1 h, allowing the formation of covalent bonds between the thiol groups of DTSP and the copper surface. Finally, the sensor is thoroughly rinsed with distilled water to remove any excess DTSP, leaving a functional and stable monolayer for biomolecule immobilization.

In the fourth step **(IV),** recombinant p53 protein is immobilized and selected as the bioreceptor to interact with anti-p53 antibodies. A solution of p53 protein, prepared from a

500.0 mg/mL stock in PBS (pH 7.4), is diluted to concentrations of 1.0, 2.5, 5.0, and 10.0 µg/mL for immobilization tests. A 5 µL volume of the solution is applied to the DTSP-functionalized surface and incubated at room temperature. The amino groups of the p53 protein covalently react with the N-hydroxysuccinimide (NHS) ester groups present in the DTSP, ensuring efficient immobilization. After incubation, the surface is rinsed with PBS to remove unbound proteins.

In the fifth step **(V)**, nonspecific binding sites are blocked using BSA. BSA solutions are prepared in PBS at concentrations of 0.1, 0.5, and 1.0%, and a 5 µL volume is applied to the functionalized surface. The surface is incubated for 2 h to allow BSA molecules to bind to any remaining reactive sites, preventing nonspecific binding during analyte detection. Excess BSA is removed by washing with PBS, leaving the surface ready for interaction with the target antibody.

In the sixth step **(VI)**, anti-p53 antibodies are linked to the functionalized and blocked sensor surface to evaluate specific interactions with the immobilized p53 protein. Anti-p53 antibody solutions are prepared by diluting a concentrated stock in PBS (pH 7.4) to obtain concentrations ranging from pure PBS to 1250.0 pg/mL. A controlled volume of 5 µL is carefully applied to the functionalized biosensor surface. During room temperature incubation, the antibodies specifically interact with the p53 protein through antigen-antibody recognition, forming a stable complex. This interaction induces changes in the local dielectric properties of the SUT, causing shifts in the resonance frequency (Δf_r). Here, the initial resonance shift (Δfr_1) is calculated as the difference between the resonance frequency of the surface functionalized with the DTSP monolayer (reference frequency) and the frequency recorded immediately after the application of antibodies. Its is expressed by the following equation (5-1):

$$\Delta f_{r1} = f_{reference} - f_{functionalized} \tag{5-1}$$

Subsequently, the stabilized resonance shift (Δfr_2), is evaluated, representing the difference between the frequency recorded immediately after the initial interaction and the frequency recorded after the stabilization period. This shift captures the final adjustments in the local dielectric properties and is calculated as:

$$\Delta f_{r2} = \left| f_{stabilized} - f_{functionalized} \right| \tag{5-2}$$

Finally, the total shift (Δf_T) is obtained as the sum of the two previous shifts, providing a cumulative measure of the impact of the interaction between the analyte and the functionalized surface. The corresponding formula is given by equation (5-3):

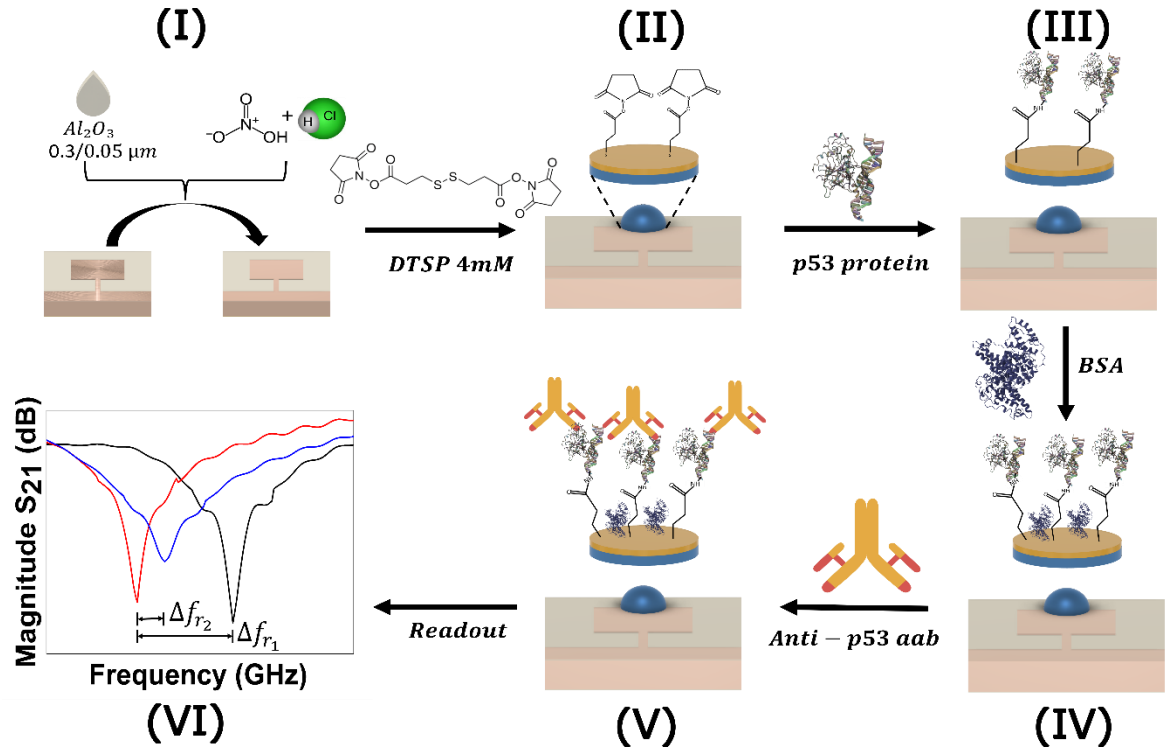

Figure 5-1. Step-by-step assembly of the microwave-based biosensor: (I) Physical abrasion of the microstrip line substrate using alumina powder (0.30 and 0.05 µm diameter), followed by sequential washing in nitric acid and hydrochloric acid to remove surface impurities and ensure optimal surface cleaning for functionalization. (II) Functionalizing the copper microstrip resonator with a 4 mM DTSP self-assembled monolayer enables covalent binding of the p53 protein as a bioreceptor. (III) Immobilization of recombinant wild-type p53 protein onto the functionalized surface to specifically interact with anti-p53 antibodies. (IV) Blocking of nonspecific binding sites using BSA. (V) Specific detection of anti-p53 antibodies through their interaction with immobilized p53 protein, producing measurable frequency shifts in the S_{21} response. (VI) The signal readout is correlated with changes in anti-p53 autoantibody concentrations. The total frequency shift is defined as $\boldsymbol{\Delta f_T = \Delta f_{r1} + \Delta f_{r2}}$, ensuring consistent analysis of functionalization and binding effects.

$$\Delta f_T = \Delta f_{r1} + \Delta f_{r2} \tag{5-3}$$

These frequency shifts allow for a detailed characterization of the biosensor's functionality, providing quantitative metrics on the device's sensitivity and specificity. The relationship between the shift values and the concentrations of anti-p53 antibodies ensures an accurate assessment of the biosensor's performance under controlled experimental conditions.

5.2.1 Optimization of the Microwave-Based Label-Free Biosensor

The optimization of the biofunctionalization of the SIR in the microwave region is essential to achieve specific and stable detection of the anti-p53 antibodies. This process includes activating and preparing the biosensor surface using different concentrations and incubation times to maximize sensitivity and minimize nonspecific interactions.

Changes in frequency from PBS and 0.1, 0.5, and 1.0% BSA as model biomolecule with incubation times of 0, 1, 2 h, and overnight was the first approach to evaluate the transducer response to (bio)molecules towards optimization of the biosensor assembly. PBS served as a stable reference medium, while BSA blocked nonspecific sites, preventing the binding of interferents. This analysis identified optimal conditions that maximize specificity without compromising the biosensor's functionality.

The study compared three surface configurations: without chemical activation, with chemical activation exposing copper structures to chemisorb biomolecules directly, and modifying with a 4 mM DTSP monolayer to link biomolecules chemically. Without chemical activation, interaction with BSA was inefficient. Chemical activation improved surface reactivity by facilitating efficient interactions with BSA, while the DTSP monolayer provided a more uniform surface, optimizing biomolecule anchoring and significantly reducing nonspecific adsorption.

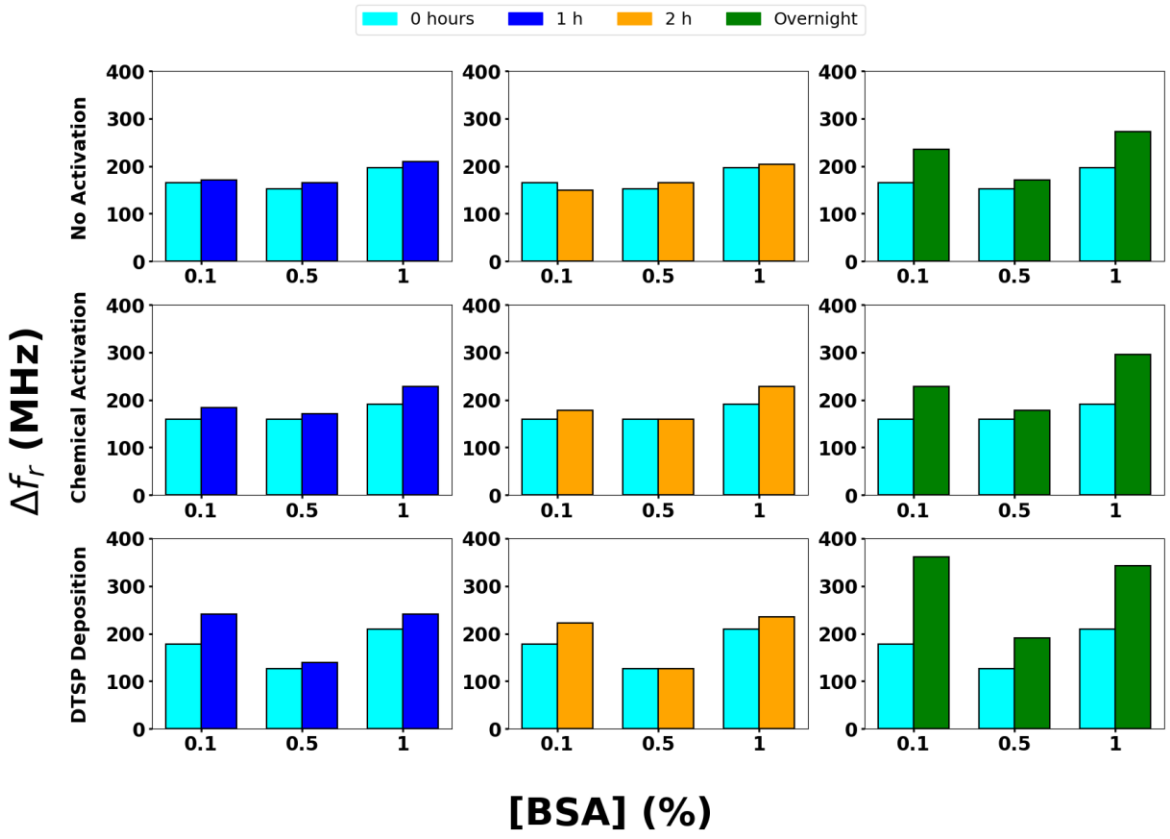

Figure 5-2. Frequency shifts (Δf) during BSA adsorption on copper surfaces: no activation, chemical activation, and DTSP modification.

The frequency shifts were moderate and consistent across different incubation times in the first row of results, corresponding to the surface without chemical activation. It suggests that, in the absence of any treatment, the sensor surface has limited reactivity and impairs

the effectiveness of BSA adsorption. Moving to the second row, where the surface was chemically activated with nitric acid (HNO_3) and hydrochloric acid (HCl), the results show a slight improvement in the transducer's response. This chemical activation removes oxides and impurities, exposing a more reactive copper surface that facilitates more efficient interactions with BSA. The frequency shifts observed here were greater than those in the non-activated configuration, reflecting a better capacity for biomolecule anchoring directly by physical adsorption.

Finally, the third row presents the results after the surface was treated with both chemical activation and a self-assembled DTSP monolayer (4 mM). In this series, all experiments used a 1.0% BSA concentration, the only variable being the treatment applied to the transducer. The sensitivity was assessed in the final column, where an overnight incubation was applied to each treatment stage. Initially, without any chemical treatment, the sensor exhibited a frequency shift of 273 MHz. After chemical activation, the frequency shift increased to 295.2 MHz, demonstrating an improved transducer response. The most significant enhancement occurred when the sensor was treated with both chemical activation and a DTSP monolayer (4 mM), resulting in a frequency shift of approximately 342.85 MHz. This last configuration showed the most significant improvement, highlighting the combined effectiveness of chemical activation and the DTSP monolayer in enhancing the transducer's response by covalently linking the protein.

Thus, the functionalization of the transducer through different treatments demonstrated how the preparation and incubation time of the copper surface directly affect the device's response. Figure 5-3 shows the frequency shifts (Δf_r) obtained as a function of incubation times (1 and 2h, and overnight) during the immobilization process of p53 protein at a concentration of 2.5 µg/mL. The results reveal that the frequency shift progressively increased with incubation time, reaching a maximum value of 276.79 MHz under overnight incubation. This behavior suggests that the more extended the incubation periods, the greater the interaction with the p53 protein onto the functionalized microwave-based transducer surface, promoting more efficient and stable biomolecule immobilization.

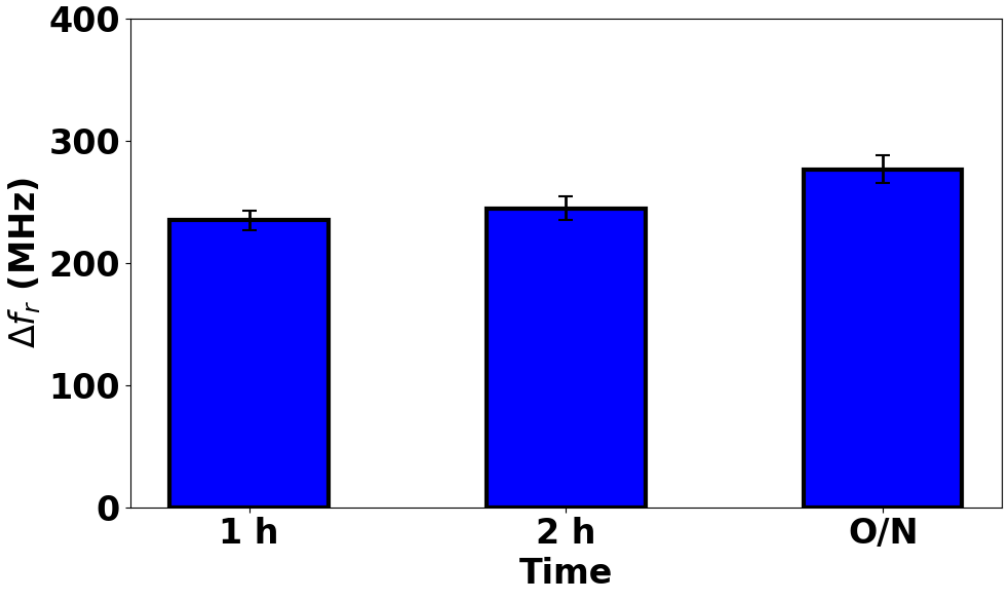

Figure 5-3. Average resonance frequency shifts ($\boldsymbol{\Delta f_r}$) as a function of p53 incubation time. Error bars were estimated from the standard deviation (n = 3).

After that, the microwave-based transducer functionalization was optimized. Figure 5-4a shows the frequency shift (Δf_r) and the signal-to-noise ratio (S/N) as a function of p53 protein concentration. The obtained results reveal that a concentration of 2.5 µg/mL provides an optimal frequency shift, reaching an average value of approximately 276.1 MHz ($\Delta f_{r,o/N}$) under overnight incubation, while for the 0-h condition ($\Delta f_{r,0h}$), an average of 211.6 MHz was obtained. This concentration stands out as it generates a significant and consistent response, surpassing lower concentrations (1.0 µg/mL) and avoiding the variability and reduced efficacy observed at higher concentrations (such as 5.0 µg/mL or more). Therefore, 2.5 µg/mL was selected as the optimal concentration for biosensor functionalization because, in this case, we obtained a high response and stability in the proposed biosensor's behavior.

The blocking with BSA at various concentrations was examined. Figure 5-4b presents the acquired results. During the biosensor blocking optimization phase, the optimum p53 concentration of 2.5 µg/mL was utilized, and various BSA concentrations (0.1, 0.5, and 1.0%) were examined with incubation durations of 0 and 2 h. Figure 5-4b shows that although the frequency shift (Δf_r) is higher with 1.0% BSA at 2 h ($\Delta f_{r,1\%}$) reaching an average of 334.9 MHz, the condition with 0.5% BSA at 2 h ($\Delta f_{r,0.5\%}$) offers a more stable and reproducible response, averaging 276.1 MHz. This stability reflects better blocking functionality, reducing nonspecific binding without saturating the biosensor surface.

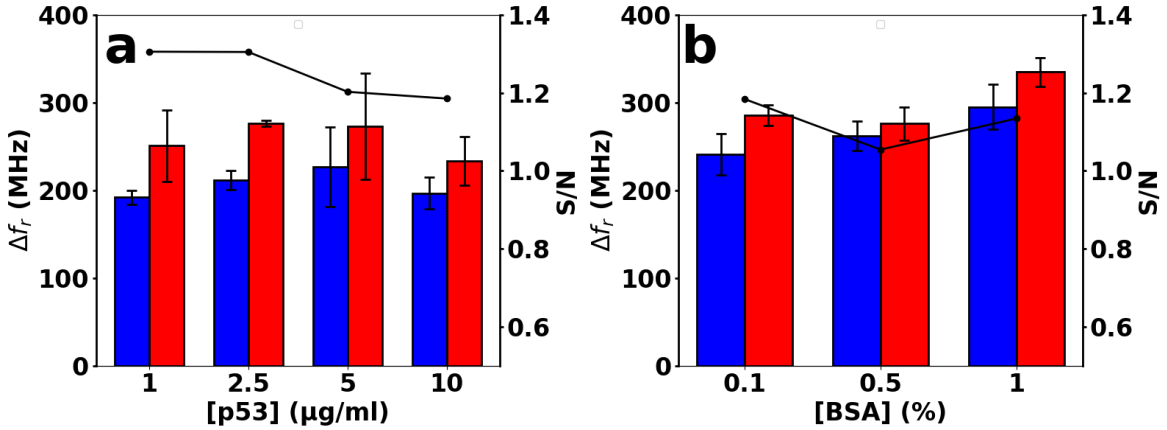

Figure 5-4. a) Frequency shifts (Δf) for different p53 protein concentrations at 0 h (blue bars) and after overnight incubation (red bars). b) Δf for different BSA blocking concentrations at 0 h (blue bars) and after 2 h incubation (red bars). The signal-to-noise ratio (S/N) is plotted on the right side of a) and b) (black line). Error bars were estimated from the standard deviation (n = 3).

5.3 Optimal Time for the Detection of Anti-p53 Antibodies

Once the functionalization and the blocking process were optimized. The resonance frequency shift (Δf_r) of the proposed transducer functionalized with a DTSP monolayer (4 mM) was evaluated in response to a fixed concentration of anti-p53 antibodies (1.0 ng/mL), considering three incubation times: 30, 45, and 60 min. The transmission S_{21} response from 4.8 to 5.8 GHz (Figs. 5-5 a-c) shows how the resonance frequency progressively changes with incubation time. In each case, the black curve corresponds to the biosensor functionalized only with DTSP, while the red and blue curves reflect the responses immediately after the addition of antibodies (0 min) and after the respective incubation times (30, 45, or 60 min).

The results show a gradual decrease in resonance frequency over time, indicating increased interaction between the anti-p53 antibodies and the proposed microwave-based transducer. The higher the incubation time, the greater the resonance frequency shift, demonstrating an increase in antibodies bound to the biosensor's functionalized surface. Likewise, the bar graph depicted in Figure 5-5d summarizes the average Δf values for each evaluated time. At 30 min, the frequency shift is 282.54 MHz, increasing to 307.94 MHz at 45 min and reaching a maximum value of 309.00 MHz after 60 min of incubation. This progressive increase suggests that the interaction between the antibodies and the biosensor improves over time, stabilizing between 45 and 60 min. The minimal difference between the values obtained at 45 and 60 min indicates that the biosensor's response approaches its maximum capacity within this interval, and 60 min was chosen for further tests.

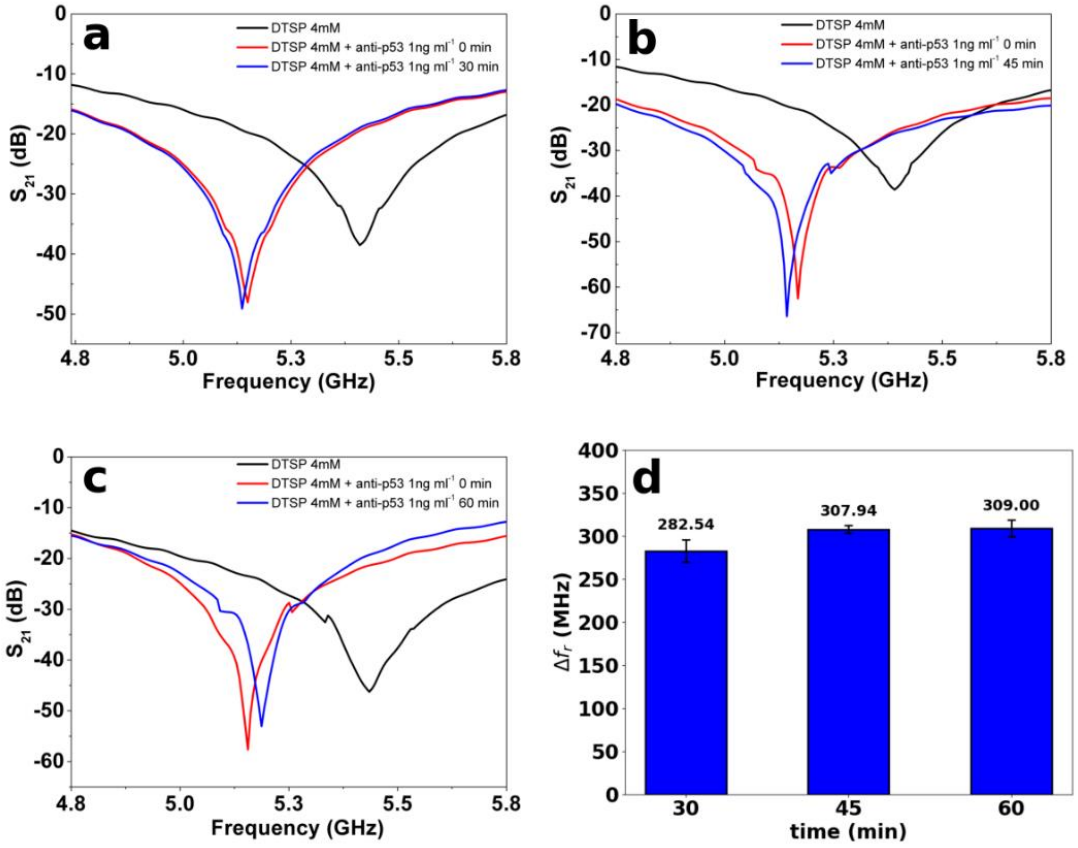

Figure 5-5. S_{21} parameter of the p53 protein-functionalized transducer (black lines) upon interaction with 1.0 ng/mL anti-p53 antibody measured immediately (red lines) and after incubation (blue lines) for a) 30, b) 45, and c) 60 min. d) Average resonance frequency shifts ($\boldsymbol{\Delta f_r}$) as a function of interaction time. Error bars were estimated from the standard deviation (n = 3).

5.4 Linear Working Range and Sensitivity

The efficacy of the developed microwave-based biosensor in distinguishing anti-p53 antibodies at varying doses was assessed. Figures 5-6 (a-f) illustrate the S_{21} parameter from 4.8 to 5.8 GHz for anti-p53 antibody concentrations of 0.0, 250.0, 500.0, 750.0, 1000.0, and 1250.0 pg/mL. Each spectrum was measured after functionalizing the sensor surface with a 4 mM DTSP monolayer. The black curves represent the baseline response of the DTSP-functionalized sensor ($f_{reference}$), indicating the initial resonance frequency before antibody addition. The red curves capture the biosensor response immediately after the application of the antibody (0 minutes). The blue curves correspond to the stabilized response after 60 minutes of incubation, representing the equilibrium frequency ($f_{stabilized}$) once the interaction has reached a steady state.

A progressive downward shift in resonance frequency (Δf_T) is observed as the concentration of anti-p53 antibodies increases. The frequency shifts are moderate at low concentrations (Figures 5-6 a-c), ranging from 206.35 MHz (PBS) to 231.59 MHz at 250.0 pg/mL and 258.20 MHz at 500.0 pg/mL. However, as the concentration increases further, more pronounced shifts are evident, such as the 285.13 MHz shift at 750.0 pg/mL (Figure 5-6e), 308.99 MHz at 1000.0 pg/mL, and 337.57 MHz at 1250.0 pg/mL (Figure 5-6f). This trend demonstrates the biosensor's ability to detect increasing analyte concentrations through cumulative changes in the dielectric environment caused by antibody binding. Figure 5-6g provides a quantitative summary of these observations, presenting the linear relationship between the frequency shift (Δf) and the concentrations of the anti-p53 antibody. The linear fit is expressed by the equation:

$$y = 0.105x + 205.933 \quad (5\text{-}4)$$

where y corresponds to the frequency shift in MHz and x to the anti-p53 concentration in pg/mL. The slope of the line, 0.105 MHz*ml/pg, reflects the biosensor's sensitivity, indicating the average change in Δf_r per unit increase in antibody concentration. The correlation coefficient (R^2 = 1.000) indicates that the linear model perfectly describes the relationship between the variables, highlighting the biosensor's consistency within this concentration range. This high degree of correlation ensures that the biosensor responds proportionally to the evaluated concentrations, allowing for precise analyte quantification. Each concentration was measured three times under identical conditions to validate the biosensor's repeatability. The results exhibited minimal variance across repeated measurements, further confirming the stability and reliability of the biosensor's performance. The small deviations observed among replicates suggest that the proposed biosensor maintains consistent behavior across multiple tests, which is critical for practical applications in biosensing.

Moreover, the linear response across from 0.0 to 1250.0 pg/mL simplifies the calibration process and allows for straightforward interpretation of results. This linear behavior ensures that the biosensor can be used to quantify unknown concentrations of anti-p53 antibodies with high accuracy, provided they fall within the calibrated range. The combination of high sensitivity, reproducibility, and linear response underscores the robustness of the proposed sensor for detecting and quantifying specific biomarkers in complex biological samples.

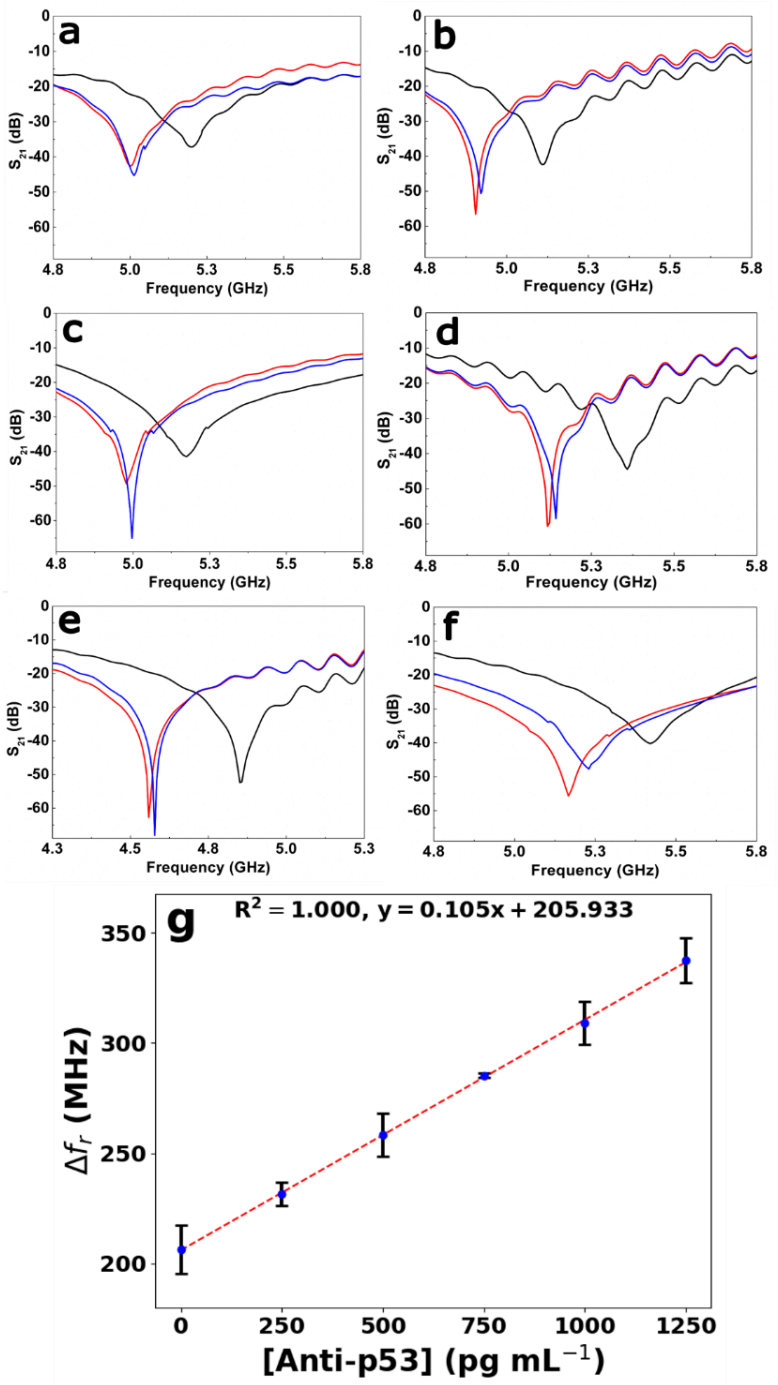

Figure 5-6. (a-f) S_{21} parameter of the p53 protein-functionalized transducer (black lines) evaluated with a) PBS, b) 250.0, c) 500.0, d) 750.0, e) 1000.0, and f) 1250.0 pg/mL of anti-p53 antibodies measured immediately upon adding the antibody solution (red lines) and after 1h interaction (blue lines). g) Resultant calibration curve of the anti-p53 antibodies concentration-dependent $\boldsymbol{\Delta f}$. Error bars were estimated from the standard deviation (n = 3).

5.5 Specificity and Selectivity, Correlation with ELISA, and Time Stability

5.5.1 Specificity and Selectivity

After evaluating the biosensor's sensitivity, this section delves into three critical aspects of its performance. First, the biosensor's specificity and selectivity are thoroughly analyzed by exposing the device to various analytes commonly found in complex biological matrices. It includes assessing its response to anti-p53 antibodies in buffered solutions containing individual interferents such as IL-6, IL-8, anti-IL-6, anti-IL-8, anti-IgG, β-1,4-GalT-V, glucose, and ascorbic acid (AA), as well as mixtures containing these interferents alongside anti-p53 antibodies. The resonance frequency shift (Δf_r) is a quantitative metric for determining the interaction strength between the biosensor and each analyte.

Figure 5-7 demonstrates that anti-p53 antibodies produce the most significant Δfr, approximately 36 MHz, highlighting a strong and specific interaction with the immobilized p53 protein layer. In contrast, individual interferents, such as IL-6 and IL-8, generated minimal Δfr values (2–4 MHz), suggesting negligible nonspecific binding. Moderate shifts (5–10 MHz) observed for anti-IgG and β-1,4-GalT-V can be attributed to weak nonspecific interactions, while chemical species like glucose and AA result in shifts below 3 MHz, confirming the biosensor's ability to discriminate between the target analyte and structurally diverse interferents. Statistical analysis further revealed statistically significant differences ($p < 0.05$) between the Δfr generated by anti-p53 antibodies alone and those from interferents tested individually, confirming the biosensor’s specificity. When exposed to a mixture of all interferents with anti-p53 antibodies, the sensor exhibited a Δfr of 41 MHz, slightly higher than the response to alone anti-p53 antibodies. This consistent response underscores the robustness of the p53 functionalized layer and its antifouling properties, even in the presence of complex biological matrices. Additionally, Δfr generated by anti-p53 antibodies alone and coexisting with all interferents showed non-significant differences ($p > 0.05$), confirming the biosensor’s selectivity.

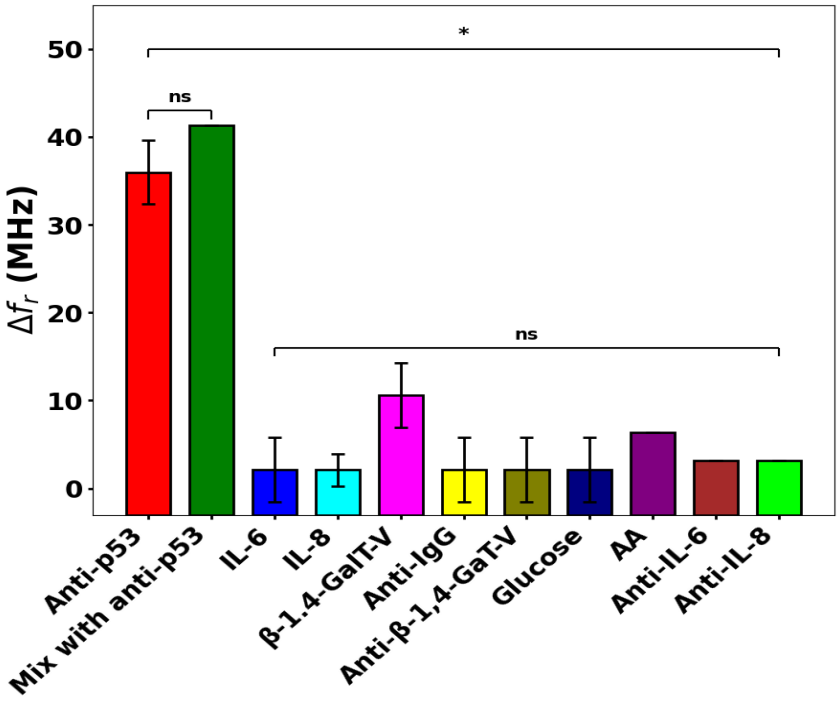

Figure 5-7. Frequency shifts (Δf) of the microwave-based biosensor for the anti-p53 antibodies target analyte in the presence of IL-6, IL-8, anti-IgG, β-1,4-GalT-V, glucose, and ascorbic acid (AA) potential interferents alone (red bar) or coexisting in a mixture (green bar). *Indicates statistically significant differences ($p < 0.05$), and ns indicates non-significant differences ($p > 0.05$)

5.5.2 Comparative Analysis Between ELISA and the Microwave-based Biosensor and Practical Application

The standard ELISA technique was used as a reference to validate the biosensor's ability to detect anti-p53 antibodies in a medical context. This method, commercially available (Pharmacell, Immunotech, Marseille, France), employs microtiter plates coated with wild-type recombinant p53 proteins (Portefaix et al., 2002). The protocol begins with diluting various blood serum samples at a 1:100 ratio, then incubating for 1 h with the immobilized proteins on the plates. Subsequently, a secondary antibody conjugated with peroxidase (HRP), designed to detect bound human IgG, is added and incubated for another h. The signal is generated using a chromogenic substrate such as TMB, resulting in a color change proportional to the concentration of anti-p53 antibodies. The color intensity is measured spectrophotometrically at 490 nm. Additionally, an inhibition assay was included as a control to ensure that the detected signals were specific to the interaction with p53, minimizing interference from other serum components.

The practical application of the biosensor was further evaluated under real conditions. The correlation between the biosensor responses and the ELISA results is shown in Figure 5-8, where positive (p6, p9, p12, p17) and negative (N28, N23) controls were analyzed.

Positive controls, which contained high concentrations of anti-p53 antibodies, exhibited significant frequency shifts in the biosensor and intense signals in ELISA, demonstrating a high concordance between both methods. Conversely, negative controls, which lacked anti-p53 antibodies, showed frequency shifts near the baseline and minimal signals in ELISA. Statistical analysis revealed a strong positive linear relationship with a high regression coefficient (R^2 = 0.97). The equation for the best fit is $y = 0.907x + 0.078$, where y corresponds to the concentrations measured by ELISA (ng/mL) and x to the concentrations measured by the biosensor (ng/mL). It confirms that the biosensor can accurately reproduce anti-p53 concentrations. Moreover, recovery studies showed that the biosensor detects anti-p53 antibodies across varying concentrations, with recovery rates ranging from 87.2 to 97.2%, demonstrating the device reliably. The relative standard deviations (RSDs) between 1.5 and 4.3% underscore the biosensor's precision and reproducibility. These findings validate the biosensor's potential as a robust tool for clinical diagnostics, particularly in cancer detection.

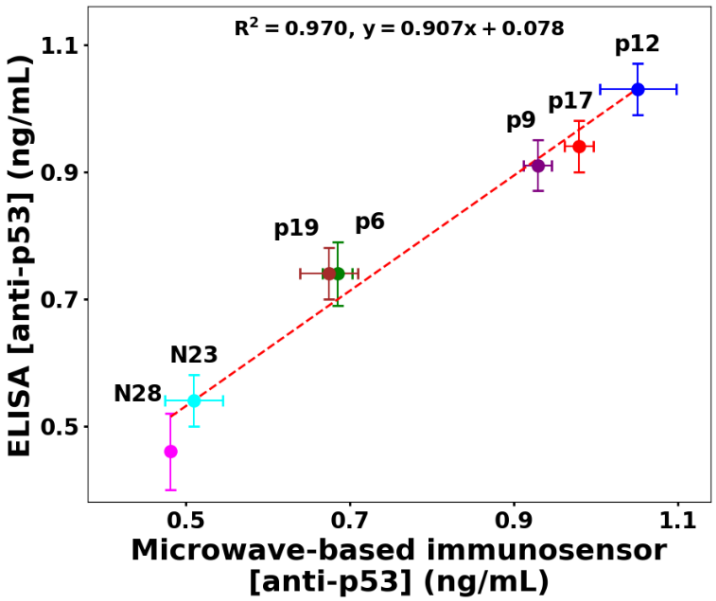

Figure 5-8. Correlation between the microwave-based biosensor and the ELISA gold standard for anti-p53 antibodies detection, using samples from different individuals. p6, p9, p12, and p17 are samples containing anti-p53 antibodies (positive controls), and N28 and N23 are samples missing the anti-p53 antibodies (negative controls), demonstrating the high agreement between the two methods.

5.5.3 Time Stability

The biosensor's operational stability was evaluated over three weeks by exposing it to a constant concentration of anti-p53 (750.0 pg/mL). The results are presented in Figure 5-9, where the initial frequency shift (Δfr) of 285 MHz at the start of the experiment can be

observed. This value remained stable during the first two weeks, with minor variations within the experimental error margin. The stabilization parameter to determine biosensor stability was three times the standard deviation above and below the measured shift at day 1 (week = 0) (upper and lower dashed lines in the figure). This criterion established an acceptable range of variations to classify the biosensor as stable. During the first two weeks, all Δfr values remained within this range, indicating reliable and consistent performance. However, from the third week onwards, the frequency shift significantly decreased, reaching approximately 200 MHz, falling outside the defined stability range. It suggests that although the biosensor maintains high stability in its dielectric properties during the first two weeks, factors such as the degradation of the functionalized monolayer, residue accumulation on the surface, or structural integrity loss of the biomolecules could affect its sensitivity and reproducibility in the long term.

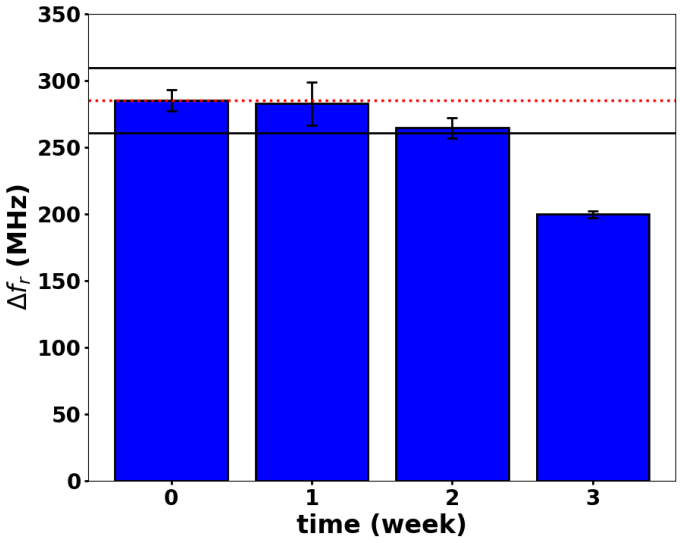

Figure 5-9. Time stability study of the microwave-based biosensor to detect 750.0 pg/ml of anti-p53 antibodies. Error bars were estimated as the standard deviation (n = 3).

5.5.4 Limit of detection (LOD)

In this study, the LOD was calculated using the blank's standard deviation and the calibration curve's slope obtained from the sensitivity analysis based on the following equation:

$$LOD = \frac{3 * \sigma_{blank}}{m} \quad (5\text{-}5)$$

Where:

- The standard deviation of the blank (σ_{blank}) was derived from the signal in the absence of the analyte, represented in this case by the PBS buffer.

- The calibration curve (*m*) slope was calculated from the linear fit of the frequency shifts (Δf_r) as a function of anti-p53 concentration.

As a result of this calculation, described in Equation 5-5, a LOD of 315.29 pg/mL was determined, indicating the minimum concentration of anti-p53 that the sensor can reliably detect. This minimum threshold for performing reliable quantitative measurements of anti-p53 highlights the biosensor's ability to detect low concentrations of anti-p53, comparable to standard techniques, but with the advantage of being a fast, non-invasive, and label-free method. These results reflect the biosensor's suitability for diagnostic and monitoring applications, emphasizing its potential as a low-cost and easy-to-implement tool for biomarker detection at early stages of disease.

6. Conclusions and perspectives

This work developed a label-free microwave-based biosensor for detecting anti-p53 antibodies and validated it with a few samples, demonstrating its potential as an innovative analytical device with significant implications for clinical diagnostics of CRC. This biosensor integrates a microwave transduction mechanism based on stepped impedance resonators within a microstrip line, leveraging resonance frequency shifts to detect changes in dielectric properties induced by specific biomolecular interactions.

The biosensor uses a DTSP self-assembled monolayer, enabling the stable and efficient immobilization of p53 bioreceptors, ensuring high specificity and sensitivity. Complementary blocking techniques using bovine serum albumin minimized nonspecific interactions, enhancing the device's reliability in complex biological matrices. Analytical evaluations revealed remarkable performance characteristics, including a linear working range from 10.0 to 1250.0 pg/mL and a 315.29 pg/mL limit of detection. These values underscore the biosensor's suitability for detecting clinically relevant concentrations of anti-p53 antibodies, particularly for early CRC diagnosis. Cross-reactivity studies confirmed the exceptional specificity and selectivity of the device. Recovery rates between 87.2 and 97.2% and relative standard deviations within 1.5 to 4.3% highlighted their reliability and reproducibility.

Comparing the results of the device in real samples with the standard ELISA method demonstrated a strong correlation, achieving a regression coefficient of 0.97, whose concordance confirms the biosensor's accuracy and reliability, offering a viable alternative to conventional analytical diagnostic tools. Positive control samples exhibited significant Δf_r values consistent with strong ELISA signals, while negative controls produced responses near the baseline, confirming the biosensor's reliability in differentiating specific analytes. In addition, the stability assessments indicated consistent performance over two weeks under controlled storage conditions, with minor variations attributed to experimental noise. A gradual decline observed in the third week emphasized the need for optimized storage

protocols to protect the biomolecules and/or periodic recalibration to extend the biosensor's operational lifespan.

Cost-effective copper-based materials in the biosensor design underscores its accessibility and scalability. Future integration of nanostructured materials or gold surfaces into the device design can enhance sensitivity and durability further, paving the way for broader clinical applications. Moreover, the biosensor's compatibility with point-of-care diagnostic systems and its label-free operation mode make it an invaluable tool for personalized healthcare and early disease detection.

7. References

Acevedo-Osorio, G., Reyes-Vera, E., & Lobato-Morales, H. (2020). Dual-Band Microstrip Resonant Sensor for Dielectric Measurement of Liquid Materials. *IEEE Sensors Journal*, *20*(22), 13371–13378. https://doi.org/10.1109/JSEN.2020.3005185

Adeniyi, O. K., Ngqinambi, A., & Mashazi, P. N. (2020). Ultrasensitive detection of anti-p53 autoantibodies based on nanomagnetic capture and separation with fluorescent sensing nanobioprobe for signal amplification. *Biosensors and Bioelectronics*, *170*, 112640. https://doi.org/10.1016/J.BIOS.2020.112640

Ali Musa Mohammed, B. (2022). *Microwave Sensing Techniques for Materials Characterisation*.

Alimenti, A., Pittella, E., Torokhtii, K., Pompeo, N., Member, S., Piuzzi, E., & Silva, E. (2023). A Dielectric Loaded Resonator for the Measurement of the Complex Permittivity of Dielectric Substrates. *IEEE TRANSACTIONS ON INSTRUMENTATION AND MEASUREMENT*, *72*, 6001009. https://doi.org/10.1109/TIM.2023.3236301

Almuhlafi, A. M., Alshaykh, M. S., Alajmi, M., Alshammari, B., & Ramahi, O. M. (2024). A Microwave Differential Dielectric Sensor Based on Mode Splitting of Coupled Resonators. *Sensors 2024, Vol. 24, Page 1020*, *24*(3), 1020. https://doi.org/10.3390/S24031020

Amanati Shahri, A., Omidvar, A. H., Pamplona Rehder, G., & Serrano, A. L. C. (2022). A Microwave-Based Microfluidic Cell Detecting Biosensor for Biological Quantification Using the Metallic Nanowire-Filled Membrane Technology. *Sensors*, *22*(9). https://doi.org/10.3390/s22093265

Balanis, C. A. (2005). *ANTENNA THEORY ANALYSIS AND DESIGN THIRD EDITION* (Third Edition). John Wiley & Sons, Inc. https://ia800501.us.archive.org/30/items/AntennaTheoryAnalysisAndDesign3rdEd/Antenna%20Theory%20Analysis%20and%20Design%203rd%20ed.pdf

Bazgir, M., & Sheikhi, A. (2024). High Q-Factor Compact Permittivity Sensor Based on Coupled SRR-ELC Metamaterial Element and Metasurfaces Shield. *IEEE Sensors Journal*, *24*(4), 4424–4431. https://doi.org/10.1109/JSEN.2023.3345477

Berketa, K., Saiapina, O., Fayura, L., Sibirny, A., Dzyadevych, S., & Soldatkin, O. (2022). Novel highly sensitive conductometric biosensor based on arginine deiminase from Mycoplasma hominis for determination of arginine. *Sensors and Actuators B: Chemical*, *367*(January), 132023. https://doi.org/10.1016/j.snb.2022.132023

Bijalwan, A., Singh, B. K., & Rastogi, V. (2021). Analysis of one-dimensional photonic crystal based sensor for detection of blood plasma and cancer cells. *Optik*, *226*. https://doi.org/10.1016/j.ijleo.2020.165994

Boruah, B. S., Gogoi, D. J., Biswas, R., Zapata-Londoño, J., Umaña-Idárraga, F., Morales-Guerra, J., Arias-Gómez, S., Valencia-Balvin, C., & Reyes-Vera, E. (2021). *Differential microwave sensor based on microstrip lines loaded with a split-ring resonator for dielectric characterization of materials You may also like Bio-Inspired Finger like Cu-Electrodes as an Effective Sensing Tool for Heavy Metal Ion in Aqueous Solution Differential microwave sensor based on microstrip lines loaded with a split-ring resonator for dielectric characterization of materials*. 12004. https://doi.org/10.1088/1742-6596/2118/1/012004

Bourjilat, A., Kourtiche, D., Sarry, F., & Nadi, M. (2016). Interdigitated electrode biosensor for DNA sequences detection. *Proceedings of the International Conference on Microelectronics, ICM*, *2016-March*, 194–197. https://doi.org/10.1109/ICM.2015.7438021

Boutry, J., Tissot, S., Ujvari, B., Capp, J. P., Giraudeau, M., Nedelcu, A. M., & Thomas, F. (2022). The evolution and ecology of benign tumors. *Biochimica et Biophysica Acta (BBA) - Reviews on Cancer*, *1877*(1), 188643. https://doi.org/10.1016/J.BBCAN.2021.188643

Bożyk, A., Krawczyk, P., Reszka, K., Krukowska, K., Kolak, A., Mańdziuk, S., Wojas-Krawczyk, K., Ramlau, R., & Milanowski, J. (2021). Correlation between KRAS, NRAS and BRAF mutations and tumor localizations in patients with primary and metastatic colorectal cancer. *Archives of Medical Science : AMS*, *18*(5), 1221. https://doi.org/10.5114/AOMS/109170

Bray Bsc, F., Laversanne, | Mathieu, Hyuna, |, Phd, S., Ferlay, J., Siegel Mph, R. L., Soerjomataram, I., Ahmedin, |, & Dvm, J. (2024). Global cancer statistics 2022: GLOBOCAN estimates of incidence and mortality worldwide for 36 cancers in 185 countries. *CA: A Cancer Journal for Clinicians*, *74*(3), 229–263. https://doi.org/10.3322/CAAC.21834

Burling, D. (2010). CT colonography standards. *Clinical Radiology*, *65*(6), 474–480. https://doi.org/10.1016/J.CRAD.2009.12.003

Chatzipetrou, M., & Zergioti, I. (2021). Digital Printing and Functionalization of Surfaces for Biosensing Applications. *IEEE Sensors Journal*, *21*(20), 22182–22189. https://doi.org/10.1109/JSEN.2021.3108703

Chen, C. W., & Chou, J. C. (2011). Potentiometric nano-grained TiO2: Ru-based nafion/uric acid biosensor. *Proceedings - International NanoElectronics Conference, INEC*, *110*, 101–102. https://doi.org/10.1109/INEC.2011.5991744

Colorectal Cancer Biomarkers. (n.d.). Retrieved January 4, 2025, from https://fightcolorectalcancer.org/facing-colorectal-cancer/colorectal-cancer-biomarkers/

Das, S., Saxena, K., Goswami, L. P., Gayathri, J., & Mehta, D. S. (2022). Mesoporous Ag–TiO2 based nanocage like structure as sensitive and recyclable low-cost SERS substrate for biosensing applications. *Optical Materials*, *125*, 111994. https://doi.org/10.1016/J.OPTMAT.2022.111994

Ebrahimi, A., Scott, J., & Ghorbani, K. (2020). Microwave reflective biosensor for glucose level detection in aqueous solutions. *Sensors and Actuators, A: Physical*, *301*. https://doi.org/10.1016/j.sna.2019.111662

Edelman, B. R., & Weiser, M. R. (2008). Endorectal Ultrasound: Its Role in the Diagnosis and Treatment of Rectal Cancer. *Clinics in Colon and Rectal Surgery*, *21*(3), 167. https://doi.org/10.1055/S-2008-1080996

Eissa, S., Alhadrami, H. A., Al-Mozaini, M., Hassan, A. M., & Zourob, M. (2021). *Voltammetric-based immunosensor for the detection of SARS-CoV-2 nucleocapsid antigen*. https://doi.org/10.1007/s00604-021-04867-1/Published

Frasconi, M., Mazzei, F., & Ferri, T. (2010). Protein immobilization at gold–thiol surfaces and potential for biosensing. *Analytical and Bioanalytical Chemistry 2010 398:4*, *398*(4), 1545–1564. https://doi.org/10.1007/S00216-010-3708-6

Fritz, C. D. L., Otegbeye, E. E., Zong, X., Demb, J., Nickel, K. B., Olsen, M. A., Mutch, M., Davidson, N. O., Gupta, S., & Cao, Y. (2023). Red-flag signs and symptoms for earlier diagnosis of early-onset colorectal cancer. *JNCI: Journal of the National Cancer Institute*, *115*(8), 909–916. https://doi.org/10.1093/JNCI/DJAD068

Gao, S., Guisán, J. M., & Rocha-Martin, J. (2022). Oriented immobilization of antibodies onto sensing platforms - A critical review. *Analytica Chimica Acta*, *1189*, 338907. https://doi.org/10.1016/J.ACA.2021.338907

Garcia Alonso, G. (2012). *Formación de nanoestructuras de silicio por evaporación térmica y pulverización catódica*.

Gatalica, Z., Vranic, S., Xiu, J., Swensen, J., & Reddy, S. (2016). High microsatellite instability (MSI-H) colorectal carcinoma: a brief review of predictive biomarkers in the era of personalized medicine. *Familial Cancer*, *15*(3), 405–412. https://doi.org/10.1007/S10689-016-9884-6/FIGURES/3

Gavrić, I., Hodžić, E., Salibašić, M., Bajramagić, S., & Kulović, E. (2024). Analysis of TP53, APC, KRAS, and MMR Genetic mutations in colorectal cancer: A review article. *Sanamed*, *00*, 64–64. https://doi.org/10.5937/sanamed0-52803

Gul, I., Zhai, S., Zhong, X., Chen, Q., Yuan, X., Du, Z., Chen, Z., Raheem, M. A., Deng, L., Leeansyah, E., Zhang, C. Y., Yu, D., & Qin, P. (2022). Angiotensin-Converting Enzyme 2-Based Biosensing Modalities and Devices for Coronavirus Detection. *Biosensors*, *12*(11). https://doi.org/10.3390/bios12110984

Guthula, L. S., Yeh, K.-T., Huang, W.-L., Chen, C.-H., Chen, Y.-L., Huang, C.-J., Chau, L.-K., Chan, M. W. Y., & Lin, S.-H. (2022). Quantitative and amplification-free detection of SOCS-1 CpG methylation percentage analyses in gastric cancer by fiber optic nanoplasmonic biosensor. *Biosensors and Bioelectronics*, *214*, 114540. https://doi.org/10.1016/j.bios.2022.114540

Hamdi, A., Nahali, A., Harrabi, M., & Brahem, R. (2023). Optimized design and performance analysis of wearable antenna sensors for wireless body area network applications. *Journal of Information and Telecommunication*, *7*(2), 155–175. https://doi.org/10.1080/24751839.2023.2179909

Hao, Y., Wang, Y., Qi, M., He, X., Zhu, Y., & Hong, J. (2019). Risk Factors for Recurrent Colorectal Polyps. *Gut and Liver*, *14*(4), 399. https://doi.org/10.5009/GNL19097

Hasbullah, H. H., & Musa, M. (2021). Gene Therapy Targeting p53 and KRAS for Colorectal Cancer Treatment: A Myth or the Way Forward? *International Journal of Molecular Sciences 2021, Vol. 22, Page 11941*, *22*(21), 11941. https://doi.org/10.3390/IJMS222111941

Hernandez, A. L., Pujari, S. P., Laguna, M. F., Santamaría, B., Zuilhof, H., & Holgado, M. (2021). Efficient Chemical Surface Modification Protocol on SiO2 Transducers Applied to MMP9 Biosensing. *Sensors 2021, Vol. 21, Page 8156*, *21*(23), 8156. https://doi.org/10.3390/S21238156

Hewitson, P., Glasziou, P., Irwig, L., Towler, B., & Watson, E. (2007). Screening for colorectal cancer using the faecal occult blood test, Hemoccult. *Cochrane Database of Systematic Reviews*, *1*. https://doi.org/10.1002/14651858.CD001216.PUB2/INFORMATION/EN

Holtedahl, K., Borgquist, L., Donker, G. A., Buntinx, F., Weller, D., Campbell, C., Månsson, J., Hammersley, V., Braaten, T., & Parajuli, R. (2021). Symptoms and signs of colorectal cancer, with differences between proximal and distal colon cancer: a prospective cohort study of diagnostic accuracy in primary care. *BMC Family Practice*, *22*(1), 1–13. https://doi.org/10.1186/S12875-021-01452-6/TABLES/6

Horvat, N., Rocha, C. C. T., Oliveira, B. C., Petkovska, I., & Gollub, M. J. (2019). MRI of Rectal Cancer: Tumor Staging, Imaging Techniques, and Management. *Radiographics*, *39*(2), 367. https://doi.org/10.1148/RG.2019180114

Hossain, M. S., Karuniawati, H., Jairoun, A. A., Urbi, Z., Ooi, D. J., John, A., Lim, Y. C., Kaderi Kibria, K. M., Mohiuddin, A. K. M., Ming, L. C., Goh, K. W., & Hadi, M. A. (2022). Colorectal Cancer: A Review of Carcinogenesis, Global Epidemiology, Current Challenges, Risk Factors, Preventive and Treatment Strategies. *Cancers 2022, Vol. 14, Page 1732*, *14*(7), 1732. https://doi.org/10.3390/CANCERS14071732

Hou, L., Huang, Y., Hou, W., Yan, Y., Liu, J., & Xia, N. (2020). Modification-free amperometric biosensor for the detection of wild-type p53 protein based on the in situ formation of silver nanoparticle networks for signal amplification. *International Journal of Biological Macromolecules*, *158*, 580–586. https://doi.org/10.1016/j.ijbiomac.2020.04.271

Houseman, B. T., Gawalt, E. S., & Mrksich, M. (2002). Maleimide-Functionalized Self-Assembled Monolayers for the Preparation of Peptide and Carbohydrate Biochips†. *Langmuir*, *19*(5), 1522–1531. https://doi.org/10.1021/LA0262304

Hsiao, Y. S., Lin, Y. T., Chen, Y. L., Tseng, H. S., Huang, T. Y., Wu, N. J., Huang, J. H., Weng, H. C., Hsu, S. C., Cheng, T. H., & Chen, C. P. (2024). Gold-decorated laser-induced graphene for wearable biosensing and joule heating applications. *Journal of the Taiwan Institute of Chemical Engineers*, *154*, 104979. https://doi.org/10.1016/J.JTICE.2023.104979

Hussain, A., Abbas, N., & Ali, A. (2022). Inkjet Printing: A Viable Technology for Biosensor Fabrication. In *Chemosensors* (Vol. 10, Issue 3). Multidisciplinary Digital Publishing Institute (MDPI). https://doi.org/10.3390/chemosensors10030103

Instituto Nacional de Cancerología-ESE. (2020). *Infografías cáncer en cifras INC 2020*. https://www.cancer.gov.co/medios-comunicacion-1/infografias/infografias-cancer-cifras-inc-2020

Irigaray, P., Newby, J. A., Clapp, R., Hardell, L., Howard, V., Montagnier, L., Epstein, S., & Belpomme, D. (2007). Lifestyle-related factors and environmental agents causing cancer: An overview. *Biomedicine & Pharmacotherapy*, *61*(10), 640–658. https://doi.org/10.1016/J.BIOPHA.2007.10.006

Ivan, M. G., Wiegersma, S., Sweelssen, J., Saalmink, M., & Boersma, A. (2011). Solid-state potentiometric biosensors for pH quantification in biological samples. *Proceedings of IEEE Sensors*, 292–295. https://doi.org/10.1109/ICSENS.2011.6127111

Iwamuro, M., Kawai, Y., Matsumoto, T., Uda, M., & Okada, H. (2015). Serum anti-p53 antibody as a tumour marker for colorectal cancer screening. *Ecancermedicalscience*, *9*. https://doi.org/10.3332/ECANCER.2015.560

Jeon, H. J., Seo, J. hyuk, Jeong, E., Son, C. Y., Rawding, P. A., Hwang, Y., Bang, S., Jang, T. min, Kubiatowicz, L. J., Hyun, S. H., Hong, S., Song, I. C., Lee, T. H., Bu, J., & Eun, H. S. (2024). Carcinoembryonic antigen-positive circulating epithelial cells as a biomarker for the diagnosis and prognosis of colorectal cancer. *Biotechnology and Bioprocess Engineering*, *29*(5), 877–889. https://doi.org/10.1007/S12257-024-00115-4/FIGURES/4

Joof, S., Aydinalp, C., Dilman, I., Akinci, M. N., Yilmaz, T., Cayoren, M., & Akduman, I. (2022). A Guideline for Complex Permittivity Retrieval of Tissue-Mimicking Phantoms From Open-Ended Coaxial Probe Response With Deep Learning. *IEEE Transactions on Microwave Theory and Techniques*, *70*(11), 5105–5115. https://doi.org/10.1109/TMTT.2022.3209701

Kai Boon, W., Zainal Abidin, Z., & Isa Ashyap, A. Y. (2021). Designing of Microwave Metamaterial Biosensor for Water Pollution Monitoring. *Journal of Electronic Voltage and Application*, *2*(2). https://doi.org/10.30880/jeva.2021.02.02.004

Kang, S. J., Park, J., Choi, G.-S., Kim, J. G., Park, J. S., Kim, H. J., Baek, J. H., Kang, B. W., Seo, A. N., Park, S.-H., Bae, B. K., Kang, M. K., & Park, S. Y. (2025). Effects of maximum dose on local control after stereotactic body radiotherapy for oligometastatic tumors of colorectal cancer. *PLOS ONE*, *20*(1), e0313438. https://doi.org/10.1371/journal.pone.0313438

Kashyap, B., & Kumar, R. (2021). Sensing Methodologies in Agriculture for Soil Moisture and Nutrient Monitoring. *IEEE Access*, *9*, 14095–14121. https://doi.org/10.1109/ACCESS.2021.3052478

Kaur, A., Kumar, P., Gupta, A., & Sapra, G. (2023). Piezoelectric Biosensors in Healthcare. *Enzyme-Based Biosensors: Recent Advances and Applications in Healthcare*, 255–271. https://doi.org/10.1007/978-981-15-6982-1_11

Kaymaz, S. V., Nobar, H. M., Sarıgül, H., Soylukan, C., Akyüz, L., & Yüce, M. (2023). Nanomaterial surface modification toolkit: Principles, components, recipes, and applications. *Advances in Colloid and Interface Science*, *322*, 103035. https://doi.org/10.1016/J.CIS.2023.103035

Khalid, W. E. F. W., Heng, L. Y., & Arip, M. N. M. (2018). Surface modification of cellulose nanomaterial for urea biosensor application. *Sains Malaysiana*, *47*(5), 941–949. https://doi.org/10.17576/jsm-2018-4705-09

Kowalska, A. A., Czaplicka, M., Nowicka, A. B., Chmielewska, I., Kędra, K., Szymborski, T., & Kamińska, A. (2022). Lung Cancer: Spectral and Numerical Differentiation among Benign and Malignant Pleural Effusions Based on the Surface-Enhanced Raman Spectroscopy. *Biomedicines*, *10*(5). https://doi.org/10.3390/biomedicines10050993

Laugsand, E. A., Brenne, S. S., & Skorpen, F. (2020). DNA methylation markers detected in blood, stool, urine, and tissue in colorectal cancer: a systematic review of paired samples. *International Journal of Colorectal Disease 2020 36:2*, *36*(2), 239–251. https://doi.org/10.1007/S00384-020-03757-X

Lee, H. J., Lee, J. H., Choi, S., Jang, I. S., Choi, J. S., & Jung, H. Il. (2013). Asymmetric split-ring resonator-based biosensor for detection of label-free stress biomarkers. *Applied Physics Letters*, *103*(5). https://doi.org/10.1063/1.4816440

Li, J., & Kuang, X. (2024). Global cancer statistics of young adults and its changes in the past decade: Incidence and mortality from GLOBOCAN 2022. *Public Health*, *237*, 336–343. https://doi.org/10.1016/J.PUHE.2024.10.033

Liu, J., Xu, Y., Liu, S., Yu, S., Yu, Z., & Low, S. S. (2022). Application and Progress of Chemometrics in Voltammetric Biosensing. In *Biosensors* (Vol. 12, Issue 7). MDPI. https://doi.org/10.3390/bios12070494

Liu, S., Tan, Q., Song, Y., Shi, Y., & Han, X. (2020). Anti-p53 autoantibody in blood as a diagnostic biomarker for colorectal cancer: A meta-analysis. *Scandinavian Journal of Immunology*, *91*(2), e12829. https://doi.org/10.1111/SJI.12829

Llamas-Garro, I., Brito-Brito, Z., Mira, F., De Melo, M. T., & Kim, J. M. (2022). Microwave Spoof Surface Plasmon Sensor for Dielectric Material Characterization. *IEEE Sensors Letters*, *6*(5). https://doi.org/10.1109/LSENS.2022.3165215

Lu, Z., Ni, W., Liu, N., Jin, D., Li, T., Li, K., Zhang, Y., Yao, Q., & Zhang, G. J. (2023). CRISPR/Cas12a-based fluorescence biosensor for detection of exosomal miR-21 derived from lung cancer. *Microchemical Journal*, *187*, 108370. https://doi.org/10.1016/J.MICROC.2022.108370

Lundin, P. M., Fiser, B. L., Blackledge, M. S., Pickett, H. L., & Copeland, A. L. (2022). Functionalized Self-Assembled Monolayers: Versatile Strategies to Combat Bacterial Biofilm Formation. *Pharmaceutics 2022, Vol. 14, Page 1613*, *14*(8), 1613. https://doi.org/10.3390/PHARMACEUTICS14081613

Luo, X. J., Zhao, Q., Liu, J., Zheng, J. B., Qiu, M. Z., Ju, H. Q., & Xu, R. H. (2021). Novel Genetic and Epigenetic Biomarkers of Prognostic and Predictive Significance in Stage II/III Colorectal Cancer. *Molecular Therapy*, *29*(2), 587–596. https://doi.org/10.1016/J.YMTHE.2020.12.017/ASSET/9B9CE752-7673-49E6-8C5D-568CEC034A7D/MAIN.ASSETS/GR1.JPG

Ma, J., Tang, J., Wang, K., Guo, L., Gong, Y., & Wang, S. (2021). Complex Permittivity Characterization of Liquid Samples Based on a Split Ring Resonator (SRR). *Sensors 2021, Vol. 21, Page 3385*, *21*(10), 3385. https://doi.org/10.3390/S21103385

Malkin, A., Chechetkin, V., Korotkov, A., & Knyazev, N. (2021). Estimation of Uncertainty of Permittivity Measurement with Transmission Line Method in the Wide Frequency Range. *2021 29th Telecommunications Forum, TELFOR 2021 - Proceedings*. https://doi.org/10.1109/TELFOR52709.2021.9653335

Mansur, H. S., Palhares, R. M., Andrade, G. I., Piscitelli Mansur, A. A., & Barbosa-Stancioli, E. F. (2009). Improvement of viral recombinant protein-based immunoassays using nanostructured hybrids as solid support. *Journal of Materials Science: Materials in Medicine*, *20*(2), 513–519. https://doi.org/10.1007/s10856-008-3606-z

Marcuello, M., Vymetalkova, V., Neves, R. P. L., Duran-Sanchon, S., Vedeld, H. M., Tham, E., van Dalum, G., Flügen, G., Garcia-Barberan, V., Fijneman, R. J., Castells, A., Vodicka, P., Lind, G. E., Stoecklein, N. H., Heitzer, E., & Gironella, M. (2019). Circulating biomarkers for early detection and clinical management of colorectal cancer. *Molecular Aspects of Medicine*, *69*, 107–122. https://doi.org/10.1016/J.MAM.2019.06.002

Matković, A. (2024). *PERMITTIVITY MEASUREMENT OF BIOLOGICAL TISSUES AND OPEN-ENDED COAXIAL PROBE MEASUREMENT METHOD ANALYSIS*.

Mattsson, V. (2024). *Digital Comprehensive Summaries of Uppsala Dissertations from the Faculty of Science and Technology 2359*. http://urn.kb.se/resolve?urn=urn:nbn:se:uu:diva-521537

Mehrotra, P., Chatterjee, B., & Sen, S. (2019a). EM-Wave Biosensors: A Review of RF, Microwave, mm-Wave and Optical Sensing. *Sensors (Basel, Switzerland)*, *19*(5), 1013. https://doi.org/10.3390/S19051013

Mehrotra, P., Chatterjee, B., & Sen, S. (2019b). EM-wave biosensors: A review of RF, microwave, mm-wave and optical sensing. In *Sensors (Switzerland)* (Vol. 19, Issue 5). MDPI AG. https://doi.org/10.3390/s19051013

Menzler, M., Ganskow, C. S. G., Ruschig, M., Moustafa, E., Sittinger, V., Lachmann, K., Wenzel, E. V., Russo, G., Klahn, P., & Gäbler, J. (2022). Testing of Diamond

Electrodes as Biosensor for Antibody-Based Detection of Immunoglobulin Protein with Electrochemical Impedance Spectroscopy. *C*, *8*(4), 74. https://doi.org/10.3390/c8040074

Michel, M., Kaps, L., Maderer, A., Galle, P. R., & Moehler, M. (2021). The Role of p53 Dysfunction in Colorectal Cancer and Its Implication for Therapy. *Cancers 2021, Vol. 13, Page 2296*, *13*(10), 2296. https://doi.org/10.3390/CANCERS13102296

Minsalud. (2021, February 4). *Incidencia del cáncer se redujo en los últimos 3 años*. https://www.minsalud.gov.co/Paginas/Incidencia-del-cancer-se-redujo-en-los-ultimos-3-anos.aspx#:~:text=Se%20estima%20que%204%20millones,lo%20mejor%20de%20sus%20vidas

Montoya-Villada, S., Morales-Guerra, J., Catano-Ochoa, D., Zapata-Londono, J., Botero-Valencia, J., Reyes-Vera, E., Montoya-Villada, S., Morales-Guerra, J., Catano-Ochoa, D., Zapata-Londono, J., Botero-Valencia, J., & Reyes-Vera, E. (2023). Design and Implementation of a 2.4-GHz Fully Integrated Butler Matrix for Smart Antenna System. *International Journal on Communications Antenna and Propagation (IRECAP)*, *13*(1), 1–9. https://doi.org/10.15866/IRECAP.V13I1.22234

Morales-Guerra, J., Umana-Idarraga, F., Giraldo-Escobar, W., Gonzalez-Valencia, E., & Reyes-Vera, E. (2021). Performance analysis of a Compact, Flexible and Biodegradable UHF RFID Tag Antenna. *2021 International Conference on Electromagnetics in Advanced Applications, ICEAA 2021*, 357–360. https://doi.org/10.1109/ICEAA52647.2021.9539617

Mrozek, P., Gorodkiewicz, E., Falkowski, P., & Hościło, B. (2021). Sensitivity analysis of single-and bimetallic surface plasmon resonance biosensors. *Sensors*, *21*(13). https://doi.org/10.3390/s21134348

Naqui, J., Damm, C., Wiens, A., Jakoby, R., Su, L., Mata-Contreras, J., & Martín, F. (2016). Transmission Lines Loaded With Pairs of Stepped Impedance Resonators: Modeling and Application to Differential Permittivity Measurements. *IEEE Transactions on Microwave Theory and Techniques*, *64*(11), 3864–3877. https://doi.org/10.1109/TMTT.2016.2610423

Nasr, A. M. H., & Sarabandi, K. (2024). A CPW Resonator for Complex Dielectric Characterization of Thin Films at W-Band. *IEEE Transactions on Instrumentation and Measurement*, *73*, 1–11. https://doi.org/10.1109/TIM.2024.3351231

Negahdary, M., & Angnes, L. (2023). Recent advances in electrochemical nanomaterial-based aptasensors for the detection of cancer biomarkers. In *Talanta* (Vol. 259). Elsevier B.V. https://doi.org/10.1016/j.talanta.2023.124548

Øines, M., Helsingen, L. M., Bretthauer, M., & Emilsson, L. (2017). Epidemiology and risk factors of colorectal polyps. *Best Practice & Research Clinical Gastroenterology*, *31*(4), 419–424. https://doi.org/10.1016/J.BPG.2017.06.004

Omam, Z. R., Nayyeri, V., Javid-Hosseini, S. H., & Ramahi, O. M. (2022). Simple and High-Sensitivity Dielectric Constant Measurement Using a High-Directivity Microstrip Coupled-Line Directional Coupler. *IEEE Transactions on Microwave Theory and Techniques*, *70*(8), 3933–3942. https://doi.org/10.1109/TMTT.2022.3183130

Ortega, F. G., Gomez, G. E., Boni, C., García, I. C., Navas, C. G., D'vries, R. F., Molina Vallejos, M. P., Serrano, M. J., Messina, G. A., Hernández, J. E., & Fernández-Baldo, M. A. (2023). Microfluidic amperometric immunosensor based on porous nanomaterial towards claudin7 determination for colorectal cancer diagnosis. *Talanta*, *251*(July 2022). https://doi.org/10.1016/j.talanta.2022.123766

Ossa-Molina, O., Duque-Giraldo, J., & Reyes-Vera, E. (2021). Strain Sensor Based on Rectangular Microstrip Antenna: Numerical Methodologies and Experimental Validation. *IEEE Sensors Journal*, *21*(20), 22908–22917. https://doi.org/10.1109/JSEN.2021.3107136

Parandin, F., Heidari, F., Rahimi, Z., & Olyaee, S. (2021). Two-Dimensional photonic crystal Biosensors: A review. *Optics & Laser Technology*, *144*, 107397. https://doi.org/10.1016/J.OPTLASTEC.2021.107397

Pasquardini, L., Lunelli, L., Potrich, C., Marocchi, L., Fiorilli, S., Vozzi, D., Vanzetti, L., Gasparini, P., Anderle, M., & Pederzolli, C. (2011). Organo-silane coated substrates for DNA purification. *Applied Surface Science*, *257*, 10821–10827. https://doi.org/10.1016/j.apsusc.2011.07.112

Passos, R. R., Corsato, C. M., Donati, B. F., Fonseca, N. E., & da Silva, V. A. (2024). Methods of Measurements of Electromagnetic Characterization of Free Space Materials in the X-Band. *Journal of Microwaves, Optoelectronics and Electromagnetic Applications*, *23*(3). https://doi.org/10.1590/2179-10742024v23i3280724

Patel, A. (2020). Benign vs Malignant Tumors. *JAMA Oncology*, *6*(9), 1488. https://doi.org/10.1001/JAMAONCOL.2020.2592

Piñeros, M., Laversanne, M., Barrios, E., De, M., Cancela, C., De Vries, E., Pardo, C., & Bray, F. (2022). *An updated profile of the cancer burden, patterns and trends in Latin America and the Caribbean*. https://doi.org/10.1016/j

Pisoschi, A. M., Iordache, F., Stanca, L., Mitranescu, E., Bader Stoica, L., Geicu, O. I., Bilteanu, L., & Serban, A. I. (2024). Biosensors for Food Mycotoxin Determination: A

Comparative and Critical Review. *Chemosensors 2024, Vol. 12, Page 92*, *12*(6), 92. https://doi.org/10.3390/CHEMOSENSORS12060092

Pohanka, M. (2017). The piezoelectric biosensors: Principles and applications, a review. In *International Journal of Electrochemical Science* (Vol. 12, Issue 1, pp. 496–506). Electrochemical Science Group. https://doi.org/10.20964/2017.01.44

Portefaix, J.-M., Fanutti, C., Granier, C., Crapez, E., Perham, R., Grenier, J., Pau, B., & Rio, D. (2002). Detection of anti-p53 antibodies by ELISA using p53 synthetic or phage-displayed peptides. In *Journal of Immunological Methods* (Vol. 259). www.elsevier.comrlocaterjim

Poyatos Martinez, D., Ramos Somolinos, D., & Plaza Gallardo, B. (2021). Electromagnetic Characterization of Materials through High Accuracy Free Space Measurements. *15th European Conference on Antennas and Propagation, EuCAP 2021*. https://doi.org/10.23919/EUCAP51087.2021.9411297

Pozar, D. M. ., & Schaubert, D. . (2015). *Microstrip antennas : the analysis and design of microstrip antennas and arrays*. 431.

Prats-Alfonso, E., Sisquella, X., Zine, N., Gabriel, G., Guimerà, A., Del Campo, F. J., Villa, R., Eisenberg, A. H., Mrksich, M., Errachid, A., Aguiló, J., & Albericio, F. (2012). Cancer prognostics by direct detection of p53-antibodies on gold surfaces by impedance measurements. *Small*, *8*(13), 2106–2115. https://doi.org/10.1002/smll.201102724

Proudfoot, J., Nosjean, O., Blanchard, J., Wang, J., Besson, D., Crankshaw, D., Gauglitz, G., Hertzberg, R., Homon, C., Llewellyn, L., Neubig, R., Walker, L., & Villa, P. (2011). Glossary of terms used in biomolecular screening (IUPAC recommendations 2011). *Pure and Applied Chemistry*, *83*(5), 1129–1158. https://doi.org/10.1351/PAC-REC-09-05-03

Puumala, L. S., Grist, S. M., Morales, J. M., Bickford, J. R., Chrostowski, L., Shekhar, S., & Cheung, K. C. (2022). Biofunctionalization of Multiplexed Silicon Photonic Biosensors. *Biosensors 2023, Vol. 13, Page 53*, *13*(1), 53. https://doi.org/10.3390/BIOS13010053

Rahman, M. S., Suresh, S., & Waly, M. I. (2018). Risk Factors for Cancer: Genetic and Environment. *Bioactive Components, Diet and Medical Treatment in Cancer Prevention*, 1–23. https://doi.org/10.1007/978-3-319-75693-6_1

Ramella, C., Pirola, M., & Corbellini, S. (2021). Accurate Characterization of High-Q Microwave Resonances for Metrology Applications. *IEEE Journal of Microwaves*, *1*(2), 610–624. https://doi.org/10.1109/JMW.2021.3063247

Ramos, D., Cidrás, J., Plaza, B., Moravec, C., de la Torre, A., Frövel, M. R. K., & Poyatos, D. (2022). Novel Electromagnetic Characterization Methods for New Materials and Structures in Aerospace Platforms. *Materials 2022, Vol. 15, Page 5128*, *15*(15), 5128. https://doi.org/10.3390/MA15155128

Raveendran, A., & Raman, S. (2021). Complex Permittivity Extraction of Planar Dielectrics Using a Noninvasive Microwave Transmission Line Resonant Technique. *IEEE Transactions on Instrumentation and Measurement*, *70*. https://doi.org/10.1109/TIM.2021.3070614

Reja, S. I., Minoshima, M., Hori, Y., & Kikuchi, K. (2024). Recent advancements of fluorescent biosensors using semisynthetic probes. *Biosensors and Bioelectronics*, *247*, 115862. https://doi.org/10.1016/J.BIOS.2023.115862

Rex, D. K., Schoenfeld, P. S., Cohen, J., Pike, I. M., Adler, D. G., Fennerty, M. B., Lieb, J. G., Park, W. G., Rizk, M. K., Sawhney, M. S., Shaheen, N. J., Wani, S., & Weinberg, D. S. (2015). Quality indicators for colonoscopy. *American Journal of Gastroenterology*, *110*(1), 72–90. https://doi.org/10.1038/AJG.2014.385

Reyes-Vera, E., Acevedo-Osorio, G., Arias-Correa, M., & Senior, D. E. (2019). A submersible printed sensor based on a monopole-coupled split ring resonator for permittivity characterization. *Sensors (Switzerland)*, *19*(8). https://doi.org/10.3390/s19081936

Reyes-Vera, E., Montoya-Villada, S., Umana-Idarraga, F., Bedoya-Londono, S., Araujo-Munoz, J., & Ossa-Molina, O. (2024). High-Sensitivity Strain Sensing Using a Flexible Microstrip Antenna with Metamaterial Resonator. *IEEE Sensors Journal*. https://doi.org/10.1109/JSEN.2024.3499856

Rocchitta, G., Spanu, A., Babudieri, S., Latte, G., Madeddu, G., Galleri, G., Nuvoli, S., Bagella, P., Demartis, M. I., Fiore, V., Manetti, R., & Serra, P. A. (2016). Enzyme biosensors for biomedical applications: Strategies for safeguarding analytical performances in biological fluids. *Sensors (Switzerland)*, *16*(6). https://doi.org/10.3390/s16060780

Ross, F. A., Park, J. H., Mansouri, D., Combet, E., Horgan, P. G., McMillan, D. C., & Roxburgh, C. S. D. (2022). The role of faecal calprotectin in diagnosis and staging of colorectal neoplasia: a systematic review and meta-analysis. *BMC Gastroenterology*, *22*(1), 1–13. https://doi.org/10.1186/S12876-022-02220-1/TABLES/5

Saeidi, T., Ismail, I., Alhawari, A. R. H., & Wen, W. P. (2019). Near-field and far-field investigation of miniaturized UWB antenna for imaging of wood. *AIP Advances*, *9*(3). https://doi.org/10.1063/1.5081762/1076976

Schoen, R. E., Pinsky, P. F., Weissfeld, J. L., Yokochi, L. A., Church, T., Laiyemo, A. O., Bresalier, R., Andriole, G. L., Buys, S. S., Crawford, E. D., Fouad, M. N., Isaacs, C., Johnson, C. C., Reding, D. J., O'Brien, B., Carrick, D. M., Wright, P., Riley, T. L., Purdue, M. P., … Berg, C. D. (2012). Colorectal-Cancer Incidence and Mortality with Screening Flexible Sigmoidoscopy. *New England Journal of Medicine*, *366*(25), 2345–2357. https://doi.org/10.1056/NEJMOA1114635/SUPPL_FILE/NEJMOA1114635_DISCLOSURES.PDF

Sharif, M. S., Raj Theeng Tamang, M., Fu, C. H. Y., Baker, A., Alzahrani, A. I., & Alalwan, N. (2023). An Innovative Random-Forest-Based Model to Assess the Health Impacts of Regular Commuting Using Non-Invasive Wearable Sensors. *Sensors*, *23*(6), 3274. https://doi.org/10.3390/s23063274

Singh, G., Sharma, S., Singh, A., Diksha, Sushma, Pawan, Suman, Mohit, & Priyanka. (2022). Graphene oxide functionalized organosilane based fluorescent biosensor for detecting guanine in human urine. *Materials Chemistry and Physics*, *287*, 126130. https://doi.org/10.1016/J.MATCHEMPHYS.2022.126130

Skalitzky, M. K., Zhou, P. P., Goffredo, P., Guyton, K., Sherman, S. K., Gribovskaja-Rupp, I., Hassan, I., Kapadia, M. R., & Hrabe, J. E. (2023). Characteristics and symptomatology of colorectal cancer in the young. *Surgery*, *173*(5), 1137–1143. https://doi.org/10.1016/J.SURG.2023.01.018

Soldatkina, O. V., Soldatkin, O. O., Velychko, T. P., Prilipko, V. O., Kuibida, M. A., & Dzyadevych, S. V. (2018). Conductometric biosensor for arginine determination in pharmaceutics. *Bioelectrochemistry*, *124*, 40–46. https://doi.org/10.1016/j.bioelechem.2018.07.002

Stanley, M., Parker-Jervis, R., Skinner, J., De Graaf, S., Lindstrom, T., Cunningham, J. E., & Ridler, N. M. (2023). Determination of the Permittivity of Transmission Lines at Milli-Kelvin Temperatures. *IEEE Access*, *11*, 60626–60634. https://doi.org/10.1109/ACCESS.2023.3286374

Su, L., Naqui, J., Mata-Contreras, J., & Martín, F. (2016). Miniature microwave notch filters and comparators based on transmission lines loaded with stepped impedance resonators (SIRs). In *Micromachines* (Vol. 7, Issue 1). MDPI. https://doi.org/10.3390/mi7010001

Su, L., Zou, L., Fong, C. C., Wong, W. L., Wei, F., Wong, K. Y., Wu, R. S. S., & Yang, M. (2013). Detection of cancer biomarkers by piezoelectric biosensor using PZT ceramic resonator as the transducer. *Biosensors and Bioelectronics*, *46*, 155–161. https://doi.org/10.1016/j.bios.2013.01.074

Sundarraj, S., Rajagopal, G., Sundaramahalingam, B., Sundar, M., & Thangam, R. (2022). *Methods of Protein Detection in Cancer for Diagnosis, Prognosis and Therapy*. https://doi.org/10.5772/intechopen.101050

Suppiah, A., & Greenman, J. (2013). Clinical utility of anti-p53 auto-antibody: Systematic review and focus on colorectal cancer. *World Journal of Gastroenterology : WJG*, *19*(29), 4651. https://doi.org/10.3748/WJG.V19.I29.4651

Sur, D., Advani, S., & Braithwaite, D. (2022). MicroRNA panels as diagnostic biomarkers for colorectal cancer: A systematic review and meta-analysis. *Frontiers in Medicine*, *9*, 915226. https://doi.org/10.3389/FMED.2022.915226/BIBTEX

Tang, X., Gao, Z., Wei, J., Li, Z., Yi, Y., Yang, F., Muhammad, A., & Wang, C. (2023). An Interdigital Microwave Sensor Based on Differential Structure for Dielectric Constant Characteristics Measurement. *Sensors 2023, Vol. 23, Page 6551*, *23*(14), 6551. https://doi.org/10.3390/S23146551

Thomsen, M., Kersten, C., Sorbye, H., Skovlund, E., Glimelius, B., Pfeiffer, P., Johansen, J. S., Kure, E. H., Ikdahl, T., Tveit, K. M., Christoffersen, T., & Guren, T. K. (2016). Interleukin-6 and C-reactive protein as prognostic biomarkers in metastatic colorectal cancer. *Oncotarget*, *7*(46), 75013. https://doi.org/10.18632/ONCOTARGET.12601

Trotter, M., Juric, D., Bagherian, Z., Borst, N., Gläser, K., Meissner, T., von Stetten, F., & Zimmermann, A. (2020). Inkjet-Printing of Nanoparticle Gold and Silver Ink on Cyclic Olefin Copolymer for DNA-Sensing Applications. *Sensors 2020, Vol. 20, Page 1333*, *20*(5), 1333. https://doi.org/10.3390/S20051333

Udomsom, S., Mankong, U., Paengnakorn, P., & Theera-Umpon, N. (2021). Novel rapid protein coating technique for silicon photonic biosensor to improve surface morphology and increase bioreceptor density. *Coatings*, *11*(5), 595. https://doi.org/10.3390/COATINGS11050595/S1

Vásquez, G., Rey, A., Rivera, C., Iregui, C., & Orozco, J. (2017). Amperometric biosensor based on a single antibody of dual function for rapid detection of Streptococcus agalactiae. *Biosensors and Bioelectronics*, *87*, 453–458. https://doi.org/10.1016/j.bios.2016.08.082

Vatandoost, N., Ghanbari, J., Mojaver, M., Avan, A., Ghayour-Mobarhan, M., Nedaeinia, R., & Salehi, R. (2016). Early detection of colorectal cancer: from conventional methods to novel biomarkers. *Journal of Cancer Research and Clinical Oncology*, *142*(2), 341–351. https://doi.org/10.1007/S00432-015-1928-Z/METRICS

Vergnano, A., Godio, A., Raffa, C. M., Chiampo, F., Tobon Vasquez, J. A., & Vipiana, F. (2020). Open-ended coaxial probe measurements of complex dielectric permittivity in

diesel-contaminated soil during bioremediation. *Sensors (Switzerland)*, *20*(22), 1–16. https://doi.org/10.3390/s20226677

Villada, S. M., Reyes-Vera, E., & Arias-Correa, M. (2023). AnIMAGE: A MATLAB-based tool for generating microstrip antennas with complex shapes. *SoftwareX*, *23*, 101502. https://doi.org/10.1016/J.SOFTX.2023.101502

Wang, H., Tian, T., & Zhang, J. (2021). Tumor-Associated Macrophages (TAMs) in Colorectal Cancer (CRC): From Mechanism to Therapy and Prognosis. *International Journal of Molecular Sciences 2021, Vol. 22, Page 8470*, *22*(16), 8470. https://doi.org/10.3390/IJMS22168470

Wu, H. W. (2016). Label-Free and Antibody-Free Wideband Microwave Biosensor for Identifying the Cancer Cells. *IEEE Transactions on Microwave Theory and Techniques*, *64*(3), 982–990. https://doi.org/10.1109/TMTT.2016.2515098

Yang, C., & Huang, H. (2021). Extraction of Stable Complex Permittivity and Permeability of Low-Loss Materials from Transmission/Reflection Measurements. *IEEE Transactions on Instrumentation and Measurement*, *70*. https://doi.org/10.1109/TIM.2020.3047490

Yeh, C.-T., Barshilia, D., Hsieh, C.-J., Li, H.-Y., Hsieh, W.-H., & Chang, G.-E. (2021). Rapid and Highly Sensitive Detection of C-Reaction Protein Using Robust Self-Compensated Guided-Mode Resonance BioSensing System for Point-of-Care Applications. *Biosensors*, *11*(12), 523. https://doi.org/10.3390/bios11120523

Yılmaz, M., Bakhshpour, M., Göktürk, I., Pişkin, A. K., & Denizli, A. (2021). Quartz crystal microbalance (Qcm) based biosensor functionalized by her2/neu antibody for breast cancer cell detection. *Chemosensors*, *9*(4). https://doi.org/10.3390/chemosensors9040080

Zapata-Londoño, J., Umaña-Idárraga, F., Morales-Guerra, J., Arias-Gómez, S., Valencia-Balvin, C., & Reyes-Vera, E. (2021). Differential microwave sensor based on microstrip lines loaded with a split-ring resonator for dielectric characterization of materials. *Journal of Physics: Conference Series*, *2118*(1). https://doi.org/10.1088/1742-6596/2118/1/012004

Zhou, Y., Lu, Y., Liu, Y., Hu, X., & Chen, H. (2023). Current strategies of plasmonic nanoparticles assisted surface-enhanced Raman scattering toward biosensor studies. *Biosensors and Bioelectronics*, *228*, 115231. https://doi.org/10.1016/J.BIOS.2023.115231

Zhou, Y., Wang, Z., Yue, W., Tang, K., Ruan, W., Zhang, Q., & Liu, L. (2009). Label-free detection of p53 antibody using a microcantilever biosensor with piezoresistive

readout. *Proceedings of IEEE Sensors*, *December*, 819–822. https://doi.org/10.1109/ICSENS.2009.5398558

Zub, K., Hoeppener, S., Schubert, U. S., Zub, K., Hoeppener, S., & Schubert, U. S. (2022). Inkjet Printing and 3D Printing Strategies for Biosensing, Analytical, and Diagnostic Applications. *Advanced Materials*, *34*(31), 2105015. https://doi.org/10.1002/ADMA.202105015